AGU PUBLICATIONS

JGR

Journal of Geophysical Research: Solid Earth

RESEARCH ARTICLE
10.1002/2014JB011200

Key Points:
- The 1797/1833 Mentawai earthquakes were much larger than the 2007 earthquakes
- The interseismic coupling pattern changed significantly after 1797
- Heterogeneity of frictional properties may cause the "supercycle" behavior

Supporting Information:
- Readme
- Table S1 and Figures S1–S37

Correspondence to:
B. Philibosian,
belle@ipgp.fr

Citation:
Philibosian, B., K. Sieh, J.-P. Avouac, D. H. Natawidjaja, H.-W. Chiang, C.-C. Wu, H. Perfettini, C.-C. Shen, M. R. Daryono, and B. W. Suwargadi (2014), Rupture and variable coupling behavior of the Mentawai segment of the Sunda megathrust during the supercycle culmination of 1797 to 1833, *J. Geophys. Res. Solid Earth*, *119*, 7258–7287, doi:10.1002/2014JB011200.

Received 16 APR 2014
Accepted 28 JUL 2014
Accepted article online 7 AUG 2014
Published online 2 SEP 2014

Rupture and variable coupling behavior of the Mentawai segment of the Sunda megathrust during the supercycle culmination of 1797 to 1833

Belle Philibosian[1,2], Kerry Sieh[3], Jean-Philippe Avouac[1], Danny H. Natawidjaja[4], Hong-Wei Chiang[5,6], Chung-Che Wu[5], Hugo Perfettini[1,7], Chuan-Chou Shen[5], Mudrik R. Daryono[8], and Bambang W. Suwargadi[4]

[1]Tectonics Observatory, Division of Geological and Planetary Sciences, California Institute of Technology, Pasadena, California, USA, [2]Now at Équipe de Tectonique et Mécanique de la Lithosphère, Institut de Physique du Globe de Paris, Paris, France, [3]Earth Observatory of Singapore, Nanyang Technological University, Singapore, Singapore, [4]Research Center for Geotechnology, Indonesian Institute of Science (LIPI), Kampus LIPI Bandung, Bandung, Indonesia, [5]High-Precision Mass Spectrometry and Environment Change Laboratory, Department of Geosciences, National Taiwan University, Taipei, Taiwan, [6]Now at the Earth Observatory of Singapore, Nanyang Technological University, Singapore, Singapore, [7]Now at IRD/ISTerre, Université Joseph Fourier, Grenoble, France, [8]Institut Teknologi Bandung, Bandung, Indonesia

Abstract We refer to periods of subduction strain accumulation beneath the Mentawai Islands, Sumatra, as "supercycles," because each culminates in a series of partial ruptures of the megathrust in its final decades. The finale of the previous supercycle comprised two giant earthquakes in 1797 and 1833 and whatever happened in between. This behavior between two great ruptures has implications for how the megathrust will behave between its more recent partial failure, during the M_w 8.4 earthquake of 2007, and subsequent large ruptures. We synthesize previously published coral microatoll records and a large new coral data set to constrain not only these two giant ruptures but also the intervening interseismic megathrust behavior. We present detailed maps of coseismic uplift during the two earthquakes and of interseismic deformation during the periods 1755–1833 and 1950–2000, as well as models of the corresponding slip and coupling on the underlying megathrust. The large magnitudes we derive (M_w 8.6–8.8 for 1797 and M_w 8.8–8.9 for 1833) confirm that the 2007 earthquakes released only a fraction of the moment released during the previous rupture sequence. Whereas megathrust behavior leading up to the 1797 and 2007 earthquakes was similar and comparatively simple, behavior between 1797 and 1833 was markedly different and more complex: several patches of the megathrust became weakly coupled following the 1797 earthquake. We conclude that while major earthquakes generally do not involve rupture of the entire Mentawai segment, they may significantly change the state of coupling on the megathrust for decades to follow, influencing the progression of subsequent ruptures.

1. Introduction

With each recent great earthquake, it has become clearer that long paleoseismic records are necessary to accurately assess the behavior of fault systems. In the case of the 2004 Aceh-Andaman earthquake and tsunami, paleoseismic and paleotsunami studies a few years after the disaster revealed that such large events occur approximately every 500 years [*Jankaew et al.*, 2008; *Monecke et al.*, 2008] and that the previous event had occurred as a doublet in the late fourteenth and mid fifteenth centuries [*Meltzner et al.*, 2010]. The consensus among scientists before the disaster had been that this long-dormant section of the Sunda megathrust did not generate great earthquakes [e.g., *McCann et al.*, 1979]. In the case of the 2011 Tohoku earthquake and tsunami, paleotsunami records had revealed just a few years before the disaster that a previous great tsunami had occurred in A.D. 869 and that such events had happened about once every 1000 years for the past few millennia [*Minoura et al.*, 2001; *Sawai et al.*, 2007]. Tragically, scientific consensus and dissemination of this information was still a few years away when the earthquake occurred. Only by obtaining long paleoseismic records may we anticipate and properly prepare for such events.

The islands above the Sunda megathrust west of Sumatra (Figure 1) provide an exceptional environment for studying past subduction megathrust behavior. In this region, the Australian and Indian plates subduct

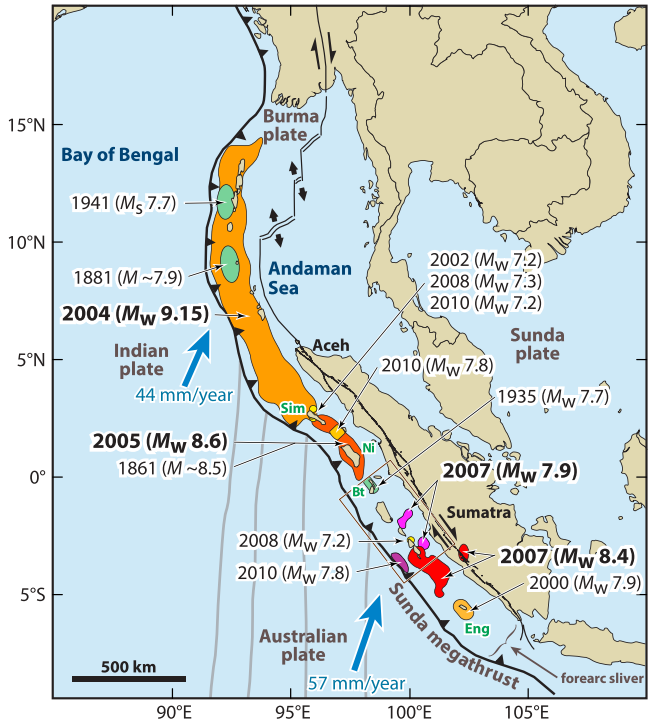

Figure 1. Map of Southeast Asia showing recent and selected historical ruptures of the Sunda megathrust. Black lines with sense of motion are major plate-bounding faults, and gray lines are seafloor fracture zones. Motions of Australian and Indian plates relative to Sunda plate are from the MORVEL-1 global model [*DeMets et al*., 2010]. The fore-arc sliver between the Sunda megathrust and the strike-slip Sumatran Fault becomes the Burma microplate farther north, but this long, thin strip of crust does not necessarily all behave as a rigid block. Sim = Simeulue, Ni = Nias, Bt = Batu Islands, and Eng = Enggano. Brown rectangle centered at 2°S, 99°E delineates the area of Figure 3, highlighting the Mentawai Islands. Figure adapted from *Meltzner et al*. [2012] with rupture areas and magnitudes from *Briggs et al*. [2006], *Konca et al*. [2008], *Meltzner et al*. [2010], *Hill et al*. [2012], and references therein.

beneath the Sunda plate. A diffuse zone of deformation west of Sumatra forms the boundary between the Australian and Indian plates, sometimes incorporated into the Capricorn microplate [*DeMets et al*., 2010]. As the islands are located above the part of the megathrust that is frictionally locked between great earthquakes, the buildup and release of tectonic strain at depth causes their cyclic subsidence and uplift [e.g., *Thatcher*, 1984]. Furthermore, the tropical environment supports the formation of coral "microatolls," which grow in the intertidal zone and track relative sea level [*Scoffin et al*., 1978]. These natural geodetic instruments contain long, high-temporal-resolution records not only of seismic fault ruptures but also of deformation between large earthquakes. For most other fault systems around the world, this level of detail is limited to the few decades of the instrumental period.

The 700 km long Mentawai section of the Sunda megathrust, between the Batu Islands and Enggano Island, is particularly interesting because it appears to be a distinct segment of the fault bounded by persistent barriers to major ruptures and characterized by rupture sequences rather than single end-to-end ruptures [*Sieh et al*., 2008]. Coral microatolls illuminate a 700 year long paleoseismic and paleogeodetic record comprising four long periods of aseismic strain accumulation, each of which culminated in a series of large megathrust ruptures. *Sieh et al*. [2008] coined the term "supercycles" for these seismic cycles that culminate in a series of large ruptures rather than in a single event. Since that time the term has been appropriated to apply more generally to situations in which a long-term cycle of strain accumulation and release encompasses a shorter-term cycle on the same fault [*Goldfinger et al*., 2013]. We prefer to limit the term to the originally intended sense, a period of strain accumulation culminating in a series of ruptures closely spaced in time. Situations in which a longer seismic cycle is superimposed on a shorter cycle, as is the case for the Tohoku region, are distinct from our definition. In the case of such "superimposed cycles," certain areas of the fault rupture at longer intervals than others, whereas at the culmination of a supercycle, *sensu stricto*, earthquakes occur in temporal clusters that are clearly interrelated.

The Mentawai segment exhibits both types of behavior, with a millennial cycle on the shallow megathrust [*Philibosian et al*., 2012] superimposed on the shorter-term supercycle of the fault patches at intermediate depth. The 2007 Mentawai earthquakes were the first large earthquakes in nearly two centuries and, judging from the past three supercycles, are the beginning of a potentially complex rupture sequence that will take place over several decades. We are motivated to study the previous supercycles because of the insights they are likely to yield about how the current rupture sequence may progress. In addition, the well-resolved Mentawai example can serve as a point of reference for comparisons with supercycle behavior elsewhere, which is being more frequently recognized as the temporal extent and precision of paleoseismic records and modern observations improve.

Sieh et al. [2008] determined that the three most recent rupture sequences occurred during the fourteenth century, during the late sixteenth to late seventeenth centuries, and during the late eighteenth and early nineteenth centuries as the historically known earthquakes of 1797 and 1833. As is common for geologic data, the paleogeodetic record from coral microatolls becomes less and less complete as one searches farther and farther back in time. Thus, out of these three, the record of the penultimate rupture sequence is the most complete. *Natawidjaja et al*. [2006] presented uplift maps and some basic forward models of megathrust slip during these events. Here we present a revised analysis of this historical supercycle, including a substantial amount of new coral data and a comprehensive review of previously published data. We synthesize all these data, first, to refine the megathrust ruptures of the 1797 and 1833 earthquakes and, second, to investigate megathrust behavior during the intervening decades. Since the first rupture in the current sequence has already occurred, the behavior of the megathrust between earlier great earthquakes is of particular interest. This analysis offers evidence that great earthquakes change the state of coupling on megathrusts and influence subsequent ruptures, vital concepts both for scientific understanding of the seismic cycle and for earthquake forecasting.

2. Methods

The upper surfaces of annually banded coral microatolls, which track relative sea level as they grow near the base of the intertidal zone, record tectonic vertical deformation. In this study, we employed now well-established techniques pioneered by *Taylor et al*. [1987] and further developed by *Zachariasen et al*. [1999, 2000], *Natawidjaja et al*. [2004, 2006, 2007], and *Meltzner et al*. [2010, 2012] to extract paleoseismic and paleogeodetic data from such microatolls. In the field, we precisely surveyed the relative elevations of microatoll surfaces before cutting radial or diametric vertical slices with a chainsaw designed for underwater cutting of concrete. Because there may be numerous specimen- or site-specific nontectonic environmental influences on coral growth, we avoided solitary specimens. Instead, we preferentially selected corals that belonged to populations with similar morphology and at similar elevations. We also place more emphasis on data that are consistent across multiple sites.

We later produced an X-ray image of each collected coral slice to illuminate the annual density bands and mapped them in cross section. To constrain the dates of growth, we determined ages of one or more small samples from each slice, using uranium-thorium disequilibrium techniques developed and described by *Edwards et al*. [1988] and *Shen et al*. [2002, 2008, 2012] (see Table S1). We sampled predominantly *Porites lutea* and *Porites lobata* species, as these form the longest-lived hemispherical colonies (all corals we present are of this type unless otherwise specified). However, we occasionally sampled other types of hemispherical colonies with larger corallites, as these have thicker aragonitic structures that frequently yield more precise U-Th ages. We tentatively identify those with 3–5 mm diameter corallites as *Goniastrea retiformis* and those with ~1 cm corallites as belonging to the genus *Favia*.

The results are time series of upward coral growth, with absolute ages constrained to within a few years to a few decades. Following *Meltzner et al*. [2010], we have made two improvements to earlier coral interpretation methodologies. First, we have refined the time series ages by using the dates of regional, nontectonic, oceanographically induced die-downs in the coral records. Second, we have calculated interseismic rates of subsidence using the most reliable subset of points on the growth curves. The following two sections describe in detail the reasons for and the details of these improved methods.

2.1. Improved Absolute Ages of Coral Records Using Oceanographic Die-Downs

One of the problems in determining precise time series is the imprecision of U-Th ages. Although exceptionally clean samples yield dates with uncertainties of only a few years, samples with abundant initial ^{230}Th commonly have uncertainties of several decades. This is certainly a problem when it is important to resolve the dates of earthquakes that are separated by only a few years or decades, as is the case for the 1797/1833 doublet. In some cases, one can use the historical dates of large earthquakes to reduce the uncertainty in the date of an event, as *Natawidjaja et al*. [2006] did. However, this typically relies on the questionable assumption that the outermost preserved band on a microatoll represents the living surface at the time of death. This is often an invalid assumption because most "fossil" microatolls are at least slightly eroded and some annual bands are missing from the outer perimeter of the sampled slice. A more reliable method of reducing age uncertainty is to correlate the coral

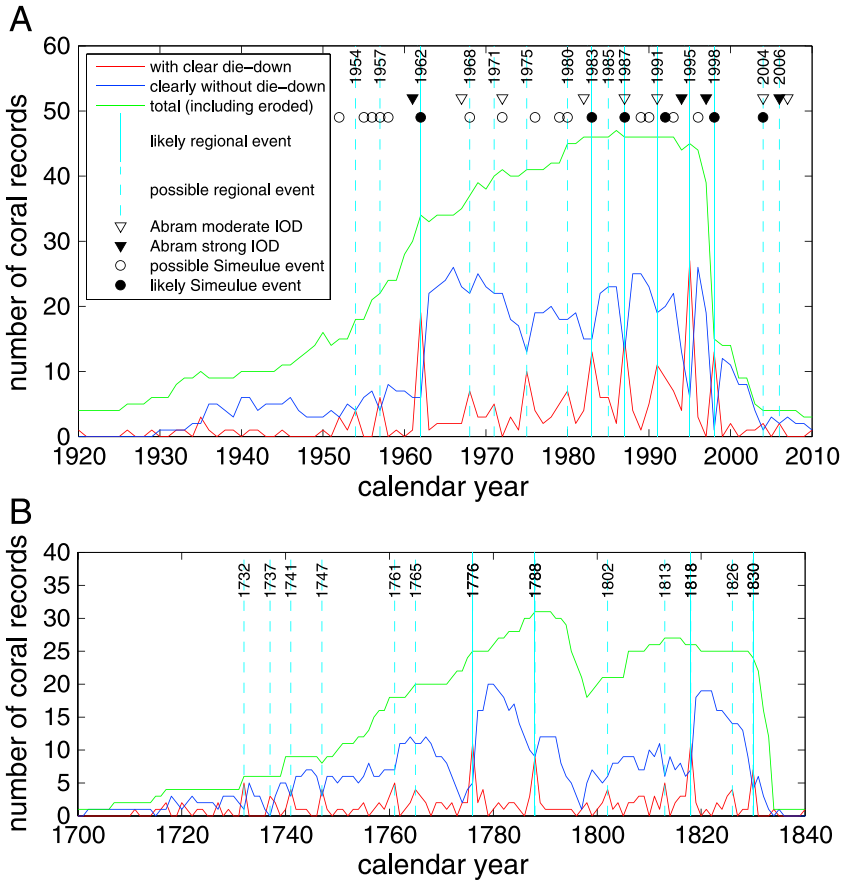

Figure 2. Oceanographic effects on coral growth expressed as widespread die-downs in certain years, likely related to positive IOD conditions. These events generally do not cause die-downs on every coral but stand out on these graphs as red spikes correlated with blue troughs. (a) Records covering the 20th and early 21st centuries, with comparison to positive IOD events identified by *Abram et al.* [2008] based on coral geochemistry. Some IOD events appear the year before the die-down occurs due to the way die-down years are assigned, but every IOD event except possibly 1972 corresponds to a die-down. About a third of the die-downs (generally the less robust ones) do not correspond to IOD events. There is also a strong correspondence with likely regional die-downs on Simeulue Island [*Meltzner et al.*, 2010, 2012]. (b) Records covering the eighteenth and early nineteenth centuries show four particularly widespread die-downs and nine less robust events. It appears that IOD events were less common during this period than in the mid- to late twentieth century.

records based on the pattern of nontectonic die-downs, events during which the upper several centimeters of the living coral surface die due to a temporary lowering of the sea surface. These events can be distinguished from tectonic uplifts based on growth morphology, as the coral will recover completely from the die-down and return to its original growth trend, rather than adjusting to a new, lower relative sea level. Because oceanographic phenomena are typically regional in scope, they can be expected to impose an isochronous marker on most or all corals over a wide area, which allows correlation between coral records.

We tested this method on twentieth-century coral records (from *Natawidjaja et al.* [2004, 2007] and our own study), which have little or no absolute age uncertainty because the outer surface was usually living when each coral was collected. Die-downs typically occur close to the beginning or ending of a calendar year, but the exact locations of the year boundaries are rarely unequivocal. We adopt the policy of assigning die-downs to the later of the two possible years (e.g., the die-down which occurred in late 1997/early 1998 is assigned to 1998). By counting the number of coral records with die-downs in each year, it is easy to identify regional die-down events (Figure 2a). We then use these events to resolve uncertainties in band counting by choosing the interpretations that allow the best correlation between die-down years among all the records.

As an additional confirmation, we compare the identified die-down events to independent measurements of the Indian Ocean Dipole (IOD). Instrumental records of the past few decades show that this oscillation, the primary non-tidal-harmonic variation of sea surface height in the Indian Ocean, can lower sea level in the Mentawai Islands by tens of centimeters in a strong positive mode [*Murtugudde et al*., 2000; *Saji et al*., 1999; *Webster et al*., 1999]. *Abram et al*. [2008] identified positive IOD events between 1845 and 2007 based on isotope geochemistry of coral records in the Mentawai region and the Seychelles. As shown in Figure 2a, almost all of the late twentieth-century IOD events are associated with coral microatoll die-downs, but there are additional interspersed die-down events which are likely due to other oceanographic phenomena that did not leave an IOD-type isotopic signature.

There is also a good correspondence between Mentawai regional die-downs and robust regional die-downs hundreds of kilometers to the north, on Simeulue Island [*Meltzner et al*., 2010, 2012]. The weaker correspondence with the less robust Simeulue events (open circles in Figure 2a) is not surprising, given that some of those represent a die-down on only one microatoll, and that IOD effects are stronger in the southern Mentawais and become weaker northward.

Based on the success of this test, we applied the same technique to the eighteenth- and nineteenth-century coral records (from *Natawidjaja et al*. [2006] and this study), using the correlations between die-downs as well as the dates of the historical earthquakes to assign a best estimate of the absolute date span of each record, within the uncertainty of the U-Th ages. As with the modern case, we were able to identify regional die-down events and adopt interpretations of band-counting uncertainties to maximize consistency among all the records. The final analysis reveals four robust regional die-downs and nine less robust events (Figure 2b), suggesting that IOD events were significantly less common between 1750 and 1830 than between 1950 and 2010. This is in and of itself an interesting result for climate science, but further investigation of IOD patterns is beyond the scope of this study.

It is worth noting that one robust regional die-down that we identify occurred in the same year (1818) as a historical tsunamigenic earthquake reported in the Bengkulu area on the coast of Sumatra [*Newcomb and McCann*, 1987]. However, unless the earthquake affected a much larger area than reported, it seems unlikely that it would have caused such a widespread coral die-down (Bengkulu is 150 km southeast of the nearest coral record we have). In fact, a contemporaneous die-down has been recognized on corals growing on Nias and Simeulue islands [*Meltzner et al*., 2014], much farther north and even less likely to have been affected by an earthquake near Bengkulu. Meltzner et al. estimate the more precise timing of the die-down to be mid-1817, consistent with our annual-scale precision, whereas the earthquake occurred in March 1818. Moreover, in every one of our coral records, the 1818 die-down has oceanographic characteristics rather than tectonic characteristics. We conclude that the 1818 die-down was largely oceanographic, and its correlation with the 1818 earthquake is coincidental. However, we cannot exclude the possibility that the die-down had a tectonic component, particularly at our southernmost sites, which are closest to Bengkulu.

Along similar lines, we do not interpret the 1962 regional die-down and subsequent recovery as a tectonic event. *Natawidjaja et al*. [2004, 2007] interpreted this event as a pair of aseismic slip pulses within a single year, the first causing uplift and the second causing an almost equal amount of subsidence. However, given that corals far to the northwest on Simeulue also experienced die-downs in 1962 [*Meltzner et al*., 2010, 2012], that the characteristics of every observed 1962 die-down are consistent with an oceanographic origin, and that a known strong positive IOD event occurred at the same time [*Abram et al*., 2008; *Saji et al*., 1999], it is likely that this was entirely or almost entirely an oceanographic event. At the very least, no tectonic event is required to explain the data.

2.2. Interseismic Rate Fitting Procedure

Rates and patterns of interseismic subsidence and uplift place important constraints on the behavior of the underlying megathrust. Over many decades, deformation at a given location can typically be approximated well by a constant linear rate. This rate can be determined from coral growth time series, but because corals respond to oceanographic fluctuations as well as land level changes, it is inappropriate to simply fit all points in the time series to obtain a rate. To choose the points to fit in order to accurately extract the interseismic signal, we must consider certain characteristics of coral growth. Upward coral growth in any one year is limited by its growth rate and the level of that year's extreme low water (ELW) [*Taylor et al*., 1987], with the species we

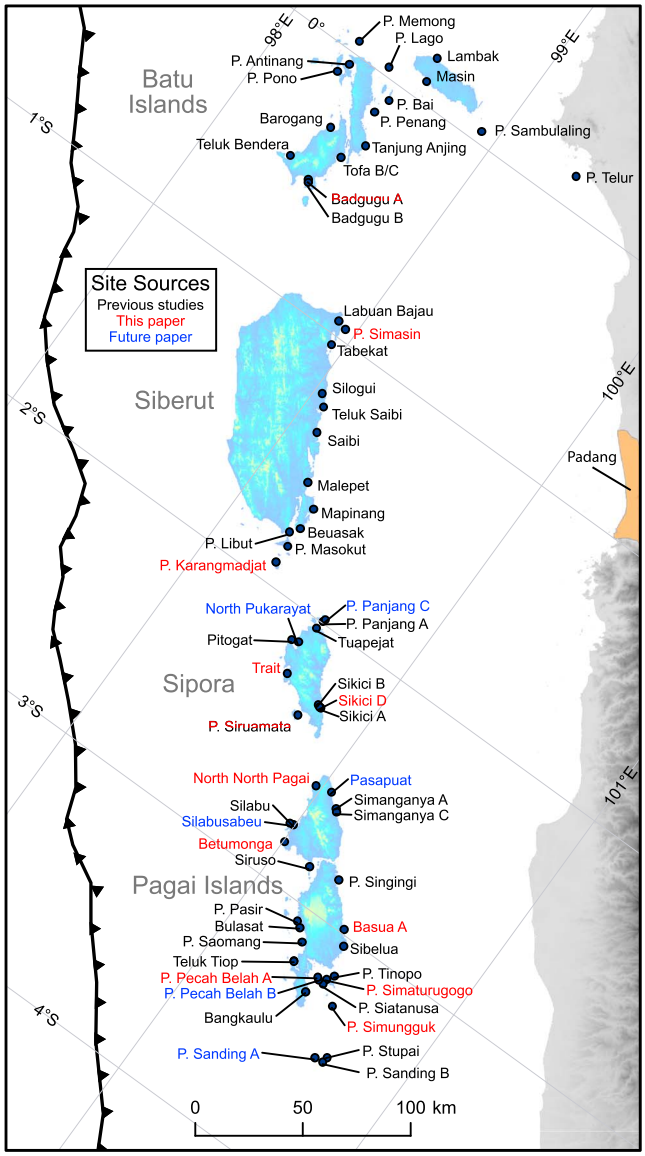

Figure 3. Index map of the Mentawai and Batu Islands showing sites used in this study. Previous studies (sites in black) comprise *Natawidjaja et al.* [2004, 2006, 2007], *Sieh et al.* [2008], and *Philibosian et al.* [2012]. Sites in red are fully presented in this paper. Some data from sites in blue are presented in this paper, but the full presentation of these sites will be in a future paper.

dominantly sample (*Porites lutea* and *lobata*) typically surviving ~20 cm above ELW in this region [*Meltzner et al.*, 2010]. This ELW-limited elevation is termed the highest level of survival (HLS), while lower growth-limited elevations are termed highest level of growth (HLG). Because of the growth-rate limitation, coral records are not sensitive to brief rises in sea level (such as negative IOD events) as they are to brief drops in sea level (such as positive IOD events), which means most recorded HLS "hits" are in years with anomalously low ELW.

Natawidjaja et al. [2006, 2007] fit combinations of preserved HLS and HLG points to obtain interseismic rates. However, these rates are biased because all of the fit points lie below the long-term trend in HLS controlled by relative mean sea level. In particular, very large die-downs early or late in the coral record (such as the 1962 and 1998 die-downs in many records) can substantially skew the results. To avoid this problem, we adopt the method of *Meltzner et al.* [2010], which is based on the idea that HLG points just before oceanographic die-downs represent the best estimates of the long-term trend in HLS. These HLG points are frequently somewhat eroded, but they are closer to the interannual average HLS than lower preserved HLG points. For our linear fits, we select the highest HLG point just before each die-down, excluding the HLG before the first die-down in a coral record if it is significantly below the trend. We calculate 2σ uncertainties on these least squares fit rates whenever there are enough points being fit (generally four or more) for the uncertainty to be meaningful. Since corals subjected to high interseismic subsidence rates typically record die-downs less frequently, uncertainties on high subsidence rates tend to be larger.

3. Coral Data and Interpreted Vertical Deformation

We now analyze coral microatolls relevant to understanding the 1797 and 1833 megathrust ruptures and interseismic behavior during adjacent time periods. In addition to consistently synthesizing all coral records from the Mentawai Islands covering the 18th and 19th centuries, we also compile all records covering the 20th and early 21st centuries. This has two purposes: first, we wish to compare recent interseismic behavior to past behavior, and, second, we obtain first-order estimates of total coseismic uplift by projecting recent interseismic subsidence rates back to the time of past earthquakes. This estimation is necessary if tectonic uplift

Table 1. Twentieth-Century Interseismic Vertical Deformation Rates

Latitude	Longitude	Full Name	Site Code	Rate (mm/yr)	Date Span
0.186	98.602	Lambak	Lm	1.5	1976–1997
0.129	99.360	P. Telur	Te	−0.2 ± 0.7	1981–1997
0.082	98.624	Masin	MSN	−0.8 ± 1.7	1952–1994
0.053	98.298	P. Memong	Mm	0.2 ± 1.2	1969–1997
0.048	98.932	P. Sambulaling	Sm	2.4 ± 1.0	1972–1997
0.039	98.460	P. Lago	Lg	2.9	1970–1997
−0.050	98.321	P. Antinang	At	−1.7	1953–1997
−0.074	98.544	P. Bai	Ba	3.2 ± 1.1	1955–1997
−0.102	98.297	P. Pono	Pn	−0.4 ± 2.7	1937–1982
−0.149	98.523	P. Penang	Pe	3.7 ± 1.5	1968–1997
−0.284	98.574	Tandjung Anjing	TAJ	−2.0 ± 4.6	1950–1997
−0.308	98.411	Barogang	BRG	−3.8 ± 0.8	1941–1997
−0.384	98.519	Tofa B/C	Tf	−0.4 ± 0.8	1949–1993
−0.500	98.345	Teluk Bendera	Tb	−8.4 ± 1.0	1955–1997
−0.549	98.471	Badgugu B	BDG-B	−6.7 ± 2.3	1935–1998
−0.942	98.912	Labuan Bajau	Lb	−1.6 ± 2.5	1954–1997
−0.953	98.956	P. Simasin	SMS	0.1 ± 0.9	1957–2010
−1.040	98.947	Tabekat	TBK	−3.9 ± 0.7	1953–1997
−1.269	99.073	Teluk Saibi	TSA	−5.4 ± 0.8	1926–1997
−1.371	99.113	Saibi	Sa	−7.3	1958–1997
−1.562	99.205	Malepet	MLP	−4.6 ± 2.0	1978–1997
−1.639	99.289	Mapinang	MPN	−7.1 ± 1.0	1958–1997
−1.737	99.292	Beuasak	Bs	−7.2 ± 0.7	1945–1998
−1.772	99.265	P. Libut	Li	−9.4 ± 4.0	1964–1997
−1.827	99.294	Masokut	MSK	−8.2 ± 5.3	1960–1997
−1.909	99.292	P. Karangmadjat	KMJ	−3.9 ± 1.9	1980–2010
−1.982	99.600	P. Panjang C	PJG-C	−6.6 ± 1.0	1971–2007
−2.033	99.592	Tuapejat	Tp	−10.5	1968–1995
−2.132	99.536	Pitogat	PTG	−7.8 ± 1.4	1970–1990
−2.289	99.802	Sikici A	SKC-A	−6.8 ± 0.9	1928–1997
−2.370	99.741	P. Siruamata	SRM	−11.5 ± 3.7	1962–1997
−2.594	100.101	Simanganya A	SMY-A	−7.4 ± 0.5	1961–1997
−2.752	99.995	Silabu	SLB	−11.5 ± 4.7	1986–2000
−2.853	100.152	P. Siruso	SRS	−10.4	1962–1994
−2.826	100.283	P. Singingi	SGG	−4.4 ± 4.7	1960–2003
−3.083	100.268	Bulasat	BLS	−10.4 ± 5.2	1961–1997
−3.039	100.463	Sibelua	SBL	−3.5	1955–1996
−3.163	100.505	P. Tinopo	TNP	−4.6 ± 2.9	1973–1993
−3.216	100.487	P. Siatanusa	STN	−5.5	1950–1994
−3.285	100.446	Bangkaulu	BKL	−6.4 ± 3.4	1980–2003
−3.268	100.572	P. Simungguk	SGK	−3.7 ± 1.7	1981–2007
−3.455	100.679	P. Stupai	STP	−9.7 ± 2.7	1950–1994
−3.481	100.677	P. Sanding B	SDG-B	−8.1 ± 2.3	1951–1994

killed the corals completely, as was the case everywhere for the 1833 earthquake and in the northern Mentawais for the 1797 earthquake. We supplement coral records from *Natawidjaja et al.* [2004, 2006, 2007], *Sieh et al.* [2008], and *Philibosian et al.* [2012] with new data from 2 old sites (Siruamata and Badgugu), 10 complete new sites, and some data from 6 other new sites that will be completely presented in a future paper (Figure 3). In this section, we first summarize our reanalysis of previously published data, then present new data, and finally synthesize all these coral records to show the spatial patterns of coseismic and interseismic deformation. In the interests of brevity, we highlight data from only a few exemplary new sites in this text; the remainder can be found in the supporting information. Figures S1 and S2 in the supporting information show compilations of all coral time series used in this study, and all interseismic rates and coseismic uplifts derived from these records are compiled in Tables 1 and 2 (geographic coordinates are relative to WGS-84 datum).

3.1. Synthesis of Previously Published Data

We reinterpret all coral records of the relevant ages from the previous papers using the improved correlation and rate-fitting techniques described in section 2. By and large our reanalysis yields interseismic

Journal of Geophysical Research: Solid Earth

10.1002/2014JB011200

Table 2. Coseismic Uplifts and Interseismic Vertical Deformation Rates Between 1750 and 1833

Latitude	Longitude	Full Name	Site Code	Pre-1797 Rate (mm/yr)	1797 Coseismic (cm)	1797 Min	Total Coseismic (cm)[a]	1797–1833 Rate (mm/yr)	1833 Coseismic (cm)	1833 Min	Modern Rate (mm/yr)	Modern Rate Source
−0.539	98.464	Badgugu A	BDG-A	0.1	20 ± 5			−1.5	5 ± 5		−6.7 ± 2.3	near BDG-B
−1.226	99.034	Silogui A	SLG-A	−3.4 ± 1.4	96	31	96 ± 13		0		−5.4 ± 0.8	near TSA
−1.982	99.600	P. Panjang C	PJG-C	−6.5 ± 1.9	70	37	163 ± 20		90		−6.6 ± 1.0	same site
−2.123	99.565	North Pukarayat[b]	NPK	−7.7	100	93	195 ± 29		95		−7.8 ± 1.4	near PTG
−2.132	99.536	Pitogat	PTG	−8.2 ± 0.8	100	14	149 ± 25		50		−7.8 ± 1.4	same site
−2.256	99.604	Trait	TRT	−8.4 ± 0.6	100	38	263 ± 43		160		−10.0 ± 2.0	interpolation
−2.286	99.785	Sikici B	SKC-B	−3.6 ± 0.7	40	11	169 ± 14		130		−6.8 ± 0.9	near SKC-A
−2.290	99.794	Sikici D	SKC-D	−4.7 ± 3.5	40	20	175 ± 14		130		−6.8 ± 0.9	near SKC-A
−2.370	99.741	P. Siruamata	SRM	−6.9	71 ± 5			−3.9 ± 2.5	182 ± 55	26	−11.5 ± 3.7	same site
−2.564	99.976	North North Pagai	NNP					−5.4 ± 1.9	148 ± 35	35	−8.0 ± 2.0	interpolation
−2.550	100.044	Pasapuat	PSP					−4.3 ± 1.9	191 ± 9	7	−7.4 ± 0.5	near SMY-A
−2.603	100.110	Simanganya C	SMY-C		15 ± 5			−7.7 ± 1.5	152 ± 7	20	−7.4 ± 0.5	near SMY-A
−2.755	99.981	Silabusabeu[b]	SSB	−9.2 ± 0.9	80	40	288 ± 88[d]		250		−11.5 ± 4.7	near SLB
−2.752	99.995	Silabu	SLB	−9.9 ± 0.1	80 ± 10			−11.8 ± 1.5	251 ± 76	55	−11.5 ± 4.7	same site
−2.831	100.008	Betumonga	BTM	−10.7 ± 1.7	90 ± 5			−11.6 ± 4.5	254 ± 84	40	−11.5 ± 4.7	near SLB
−2.826	100.283	P. Singingi	SGG	−7.8 ± 0.6	38 ± 5			−5.0	117 ± 30	32	−4.4 ± 2.0	same site[c]
−3.067	100.246	P. Pasir	PSR	−12.1 ± 4.7	50 ± 5			−10.2 ± 4.9	209 ± 90	28	−10.4 ± 5.2	near BLS
−2.981	100.423	Basua A	BSA-A					−3.6 ± 1.5	134 ± 17	30	−5.0 ± 1.0	interpolation
−3.128	100.312	P. Saomang	SMG	−9.1 ± 2.0	28 ± 4			−11.2 ± 2.0	193 ± 17	29	−9.0 ± 1.0	interpolation
−3.039	100.463	Sibelua	SBL	−5.6 ± 1.6	38 ± 10			−6.0	59 ± 30	27	−3.5 ± 2.0	same site[c]
−3.211	100.332	Teluk Tiop	TTP		5 ± 5			−8.3	212 ± 16	54	−9.0 ± 1.0	interpolation
−3.163	100.505	P. Tinopo	TNP					−3.9	103 ± 43	27	−4.6 ± 2.9	same site
−3.207	100.451	P. Pecah Belah A	PCB-A		15 ± 5			−7.3 ± 5.4	124 ± 17	30	−6.0 ± 1.0	interpolation
−3.213	100.460	P. Pecah Belah B	PCB-B							70	−6.0 ± 1.0	interpolation
−3.192	100.486	P. Simaturugogo	STG	−4.9 ± 0.3	17	17	124 ± 21[d]		107		−5.0 ± 1.0	interpolation
−3.216	100.487	P. Siatanusa	STN					−4.2	110 ± 14	23	−5.5 ± 1.0	same site[c]
−3.285	100.446	Bangkaulu	BKL	−7.6 ± 0.7	3 ± 3			−3.8	161 ± 54	11	−6.4 ± 3.4	same site
−3.268	100.572	P. Simungguk	SGK					−2.1 ± 1.7	88 ± 28	55	−3.7 ± 1.7	same site
−3.486	100.638	P. Sanding A	SDG-A		0			−1.6	155 ± 40	50	−8.1 ± 2.3	near SDG-B

[a]Total uplift divided between the two great earthquakes based on projection of contour patterns (corals died completely in 1797, providing a minimum).
[b]Sites excluded from modeling because our interpretation is inconsistent or barely consistent with the U-Th dates.
[c]Uncertainty in rate was reduced based on interpolation.
[d]Adjusted for interearthquake rate different from modern rate.

rates and coseismic uplifts that differ only slightly from those previously published and are within previously estimated uncertainties. However, a handful of our revisions are more significant and warrant more specific explanation here.

At Sikici site B on Sipora, the coral SKC03-B3 was interpreted by *Natawidjaja et al*. [2006] and *Sieh et al*. [2008] to have died in 1833, despite an age uncertainty that was large enough to encompass death in either 1797 or 1833. Based on the correlation techniques described above and new data from the nearby Sikici site D that record uplift and death of a large population of precisely dated corals in 1797 (see Figures S6 and S7), we now interpret SKC03-B3 as having died in 1797. Uplift in 1833 is not recorded at Sikici since the reefs apparently died completely in 1797.

In the coral record SMY03-C4 from Simanganya on North Pagai, *Natawidjaja et al*. [2006] and *Sieh et al*. [2008] attribute the final death of the colony to 1833 uplift and a tiny 5 cm die-down (indistinguishable from small nontectonic die-downs) to 1797 uplift. However, there is a larger $>$10 cm die-down about 8 years earlier which clearly offsets the interseismic trend. The earlier studies presumably did not assign this more obviously tectonic uplift to 1797 because there appeared to be more than 37 years of growth between it and the death of the colony. In actuality the banding in the outer part of the coral head is quite unclear. We assign the $>$10 cm uplift to 1797 and count a smaller number of bands in the outer half of the head based on correlations of oceanographic die-downs.

Zachariasen et al. [1999] and *Natawidjaja et al*. [2006] presented a total of five coral records covering the eighteenth and nineteenth centuries from Silabu on North Pagai: SLB00-A2, which died for nontectonic reasons in the mid-1700s; SLB00-A4, which died in 1797; SLB00-A3, which had a large die-down in 1797 and died completely in 1833; and NP94-A8 and A9, which hit HLS after 1797 and died in 1833. However, the scenario for this site presented by *Natawidjaja et al*. [2006] has unexplained internal inconsistencies. We favor a different interpretation of the site history which is detailed in Figure S3. Our new interpretation does not change the coseismic uplift estimates but informs our calculation of interseismic subsidence rates.

At Saomang off the coast of South Pagai, *Natawidjaja et al*. [2006] and *Sieh et al*. [2008] presented the very poorly dated coral record SMG02-A2. It was unclear how this record fit into the site's history. We obtained a much more precise age, which suggests that it died due to uplift in the 1797 earthquake. In combination with the younger P96F-1 record from a microatoll which died due to 1833 uplift, these new data allowed us to determine that the 1797 uplift at Saomang was 28 ± 4 cm, much less than the 80–100 cm previously estimated based on less-certain extrapolations.

We do not include the (minimally) revised cross sections for any of the previously published coral data, except for the modern coral NP00-A1 from Simanganya (see Figure S25). The latter figure was mistakenly omitted by *Sieh et al*. [2008]; we correct that oversight by including it here.

3.2. New Data

3.2.1. Betumonga

The Betumonga site lies in a bay on the southwest corner of North Pagai Island. A large population of long-lived, mostly hat-shaped fossil microatolls (Figure 4) provides an exemplary record of interseismic deformation before and between the 1797 and 1833 earthquakes, as well as large coseismic uplift during both of those earthquakes. The hat shape of the microatolls reflects partial uplift in 1797 (which left the crown of the hat), followed by radial outward growth at a lower level (which created the hat's brim), culminating in the death of the coral colony by uplift in 1833. We sampled two of the best-preserved microatolls. One of these is hat shaped, recording the total 1797 uplift and the interseismic period between the two earthquakes. The other died completely in 1797 and thus did not record sea level following that earthquake (Figure 5).

These corals recorded a 90 ± 5 cm uplift in 1797 and at least 40 cm of uplift in 1833, in addition to fairly well-constrained interseismic subsidence rates between 1730 and 1797 and between 1797 and 1833. The pre-1797 rate derived from A1 is somewhat higher than that derived from A2 (though the uncertainties do overlap). It is possible that the A1 record has an uncorrected tilt, as the central overgrowth obscured the concentric rings which we would normally use to measure tilt. Head A1 sits 10–20 cm lower in elevation than A2, indicating that A1 settled into the substrate and might well have tilted as it settled. We calculate the pre-1797 interseismic subsidence rate based on A2 alone, since the longer record provides a more precise rate

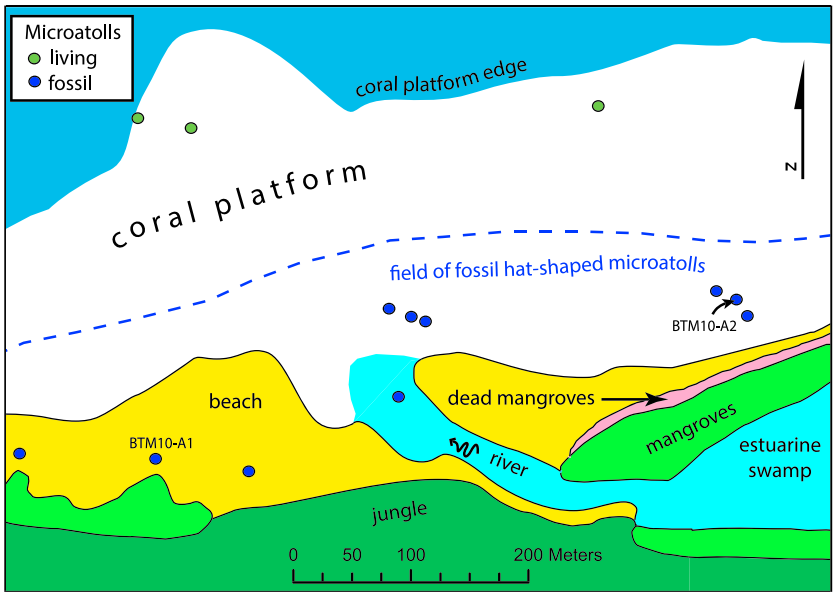

Figure 4. Map of the Betumonga site. Outflow of fresh water from the river hampers modern coral growth; only a few living colonies could be found at the far edge of the coral platform. The large field of huge microatolls that grew during the mid-1700s to early 1800s suggests that the river outlet was elsewhere (probably farther east) during that period. A perimeter of dead mangroves suggests ongoing modern subsidence at this site.

estimate and the many exposed concentric rings make it clear that A2 is untilted. The rates both before and after 1797 are ~1 cm/yr and are identical within uncertainty, illustrating that the interseismic behavior at this site did not change appreciably following the 1797 earthquake.

3.2.2. Siruamata and Bangkaulu

Siruamata is an islet off the southwest coast of Sipora Island. *Zachariasen et al*. [1999] originally presented a record from the particularly well-preserved hat-shaped microatoll Si94A-6 from a site on Siruamata's northern shore. *Natawidjaja et al*. [2006] reinterpreted this record and presented a record from a nearby modern microatoll. Si94A-6 recorded subsidence for a few decades before 1797 and a 70 cm coseismic uplift in 1797, but the outer ring that grew after 1797 was quite eroded and apparently stopped growing for nontectonic reasons prior to 1833 (perhaps due to the postulated strong IOD event in circa 1818). In order to secure a reliable sea-level history for the period between 1797 and 1833, we returned to this site in 2010 to collect a new slab (SRM10-A6) from a better-preserved radius of the same microatoll. Along this radius, the outer ring of coral continued to live and grow until 1833 (Figure 6a). The combination of the previous and the new slabs illustrates that the interseismic subsidence rate changed markedly after the 1797 earthquake, dropping almost in half from 6.9 to 3.9 mm/yr (Figure 6b).

This change in rate is intriguingly similar to the behavior at Bangkaulu, near the southeast end of South Pagai, about 150 km distant. The microatoll BKL03-A1 was uplifted and died in 1833 [*Natawidjaja et al*., 2006]. The site is near the southern terminus of the 1797 rupture, and BKL03-A1 records little or no uplift in 1797, but the interseismic subsidence rate does appear to decrease from 7.6 to 3.8 mm/yr around that time (Figure 6c). Betumonga, with no apparent rate change, lies about halfway between Siruamata and Bangkaulu.

3.2.3. Badgugu

One other coral record of particular interest comes from Badgugu A (West Badgugu), at the southeastern end of the Batu Islands. The site, microatoll cross sections, and U-Th dates were fully described by *Natawidjaja* [2003], and parts of the microatoll growth histories were included by *Natawidjaja et al*. [2006]. BDG00-A1 is an exceptionally long-lived coral head that reached a diameter of over 8 m after more than 200 years of growth (Figure 7). It emerged and died during the 1935 M_w 7.7 Batu Islands earthquake [*Natawidjaja et al*., 2004; *Rivera et al*., 2002].

Located at the northern end of both the Mentawai segment and the 1797 rupture, this coral subsided at low rates of 0–2 mm/yr throughout its life, supporting previous claims of weak coupling beneath the Batu

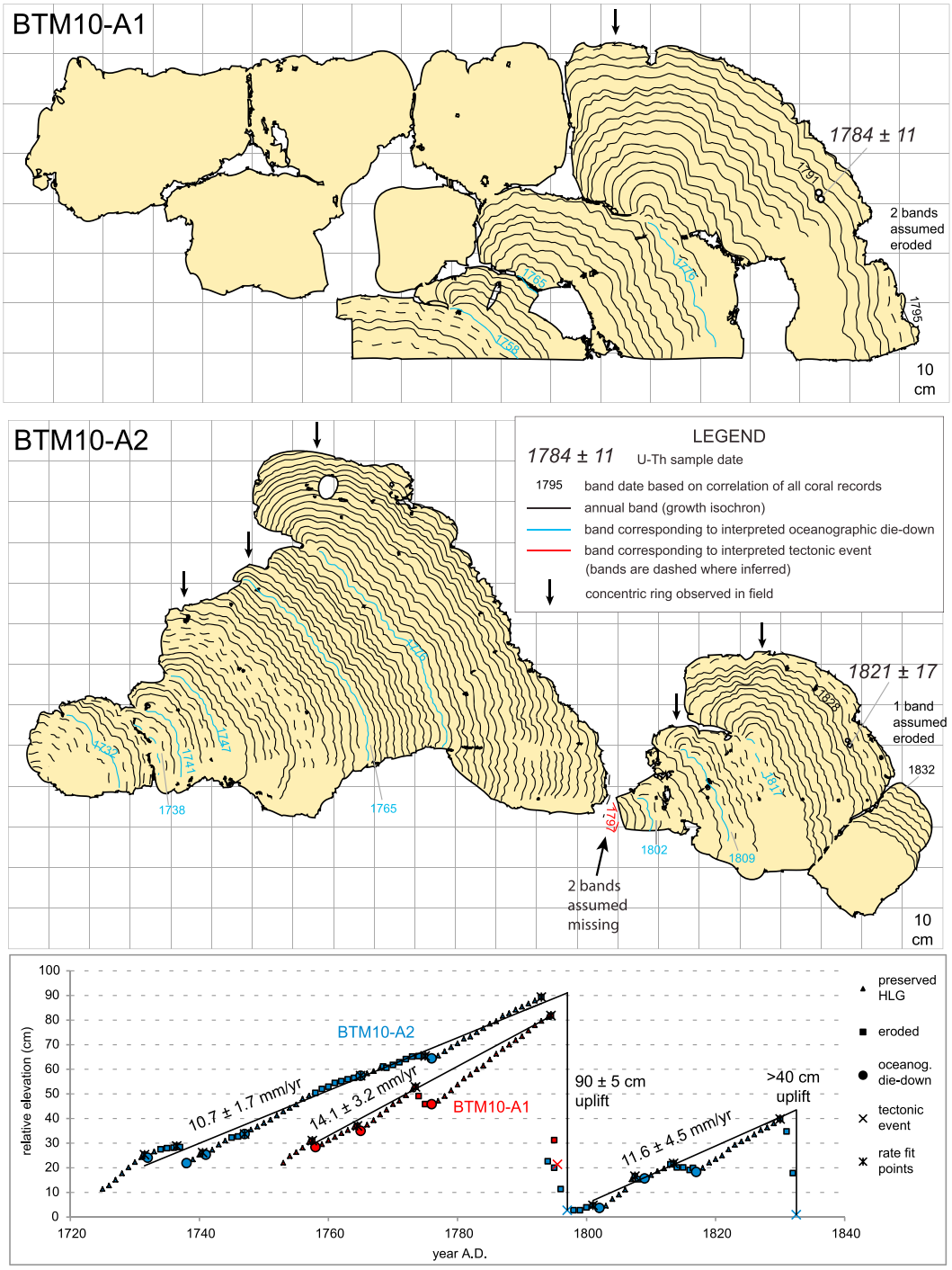

Figure 5. Slab cross sections and growth histories from Betumonga.

Islands [*Chlieh et al.*, 2008; *Natawidjaja et al.*, 2004; *Rivera et al.*, 2002]. The interseismic trend is interrupted by a 20 cm uplift in the late 1700s (presumably due to the 1797 earthquake). The post-1797 record is punctuated by numerous smaller die-downs, all of which have oceanographic characteristics and many of which correlate with geochemically-identified IOD events [*Abram et al.*, 2003]. Two of these apparently coincide with historical great earthquakes: a 5–10 cm die-down in 1833, and a 2-cm die-down in 1861 at which time an earthquake affected Nias Island to the north [*Newcomb and McCann*, 1987]. Despite the apparent coincidence, the 1833 die-down at Badgugu is likely oceanographic, as a die-down affected many

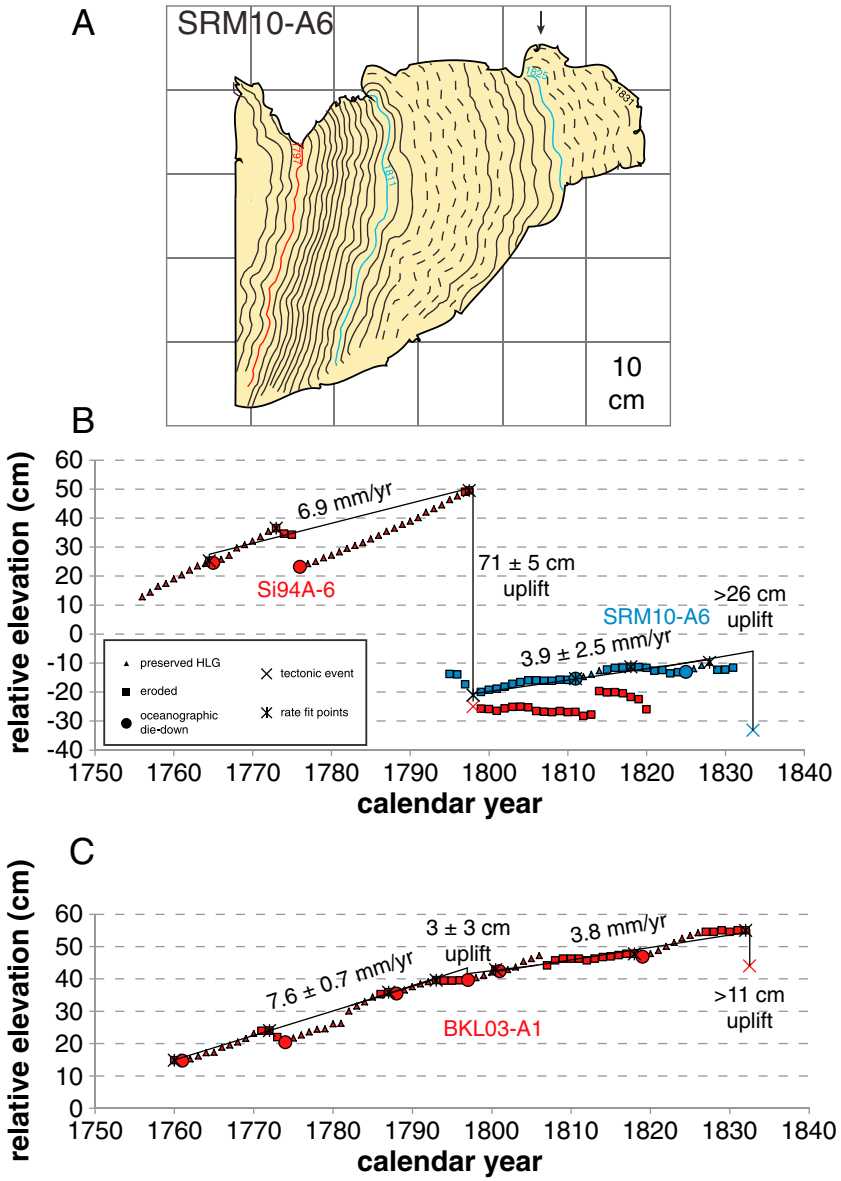

Figure 6. Coral records showing changes in subsidence rate after the 1797 earthquake. All symbols as in Figure 5. (a) Cross section of SRM10-A6 (complete outer rim of Si94A-6). (b) Growth history of two slabs from the same Siruamata microatoll. (c) Growth history of BKL03-A1 from Bangkaulu, showing a similar rate change but little to no uplift in 1797.

corals in the Nias-Simeulue region in early 1833 [*Meltzner et al.*, 2014] whereas the earthquake occurred in November. The1861 die-down is indistinguishable from the many small oceanographic die-downs that also affect this record. It is uncertain whether interseismic deformation rates at Badgugu changed following either of the great Mentawai earthquakes, but any change was clearly not large. This record demonstrates the long-term stability of the megathrust beneath the Batu Islands over an entire Mentawai supercycle and a Nias-Simeulue segment rupture in 1861[*Meltzner et al.*, 2014]. There was also no coseismic vertical deformation in the Batu Islands during the 2005 Nias-Simeulue segment rupture, except on the far-western island of Simuk [*Briggs et al.*, 2006]. Interestingly, interseismic subsidence at Badgugu increased markedly following the 1935 earthquake [*Natawidjaja et al.*, 2004], averaging 6.7 mm/yr over the period 1935–1997.

3.2.4. Additional New Sites

In addition to those discussed in the previous sections, we collected coral slabs at seven other sites in the Mentawais where the primary populations of fossil corals date to the eighteenth and nineteenth centuries: Trait

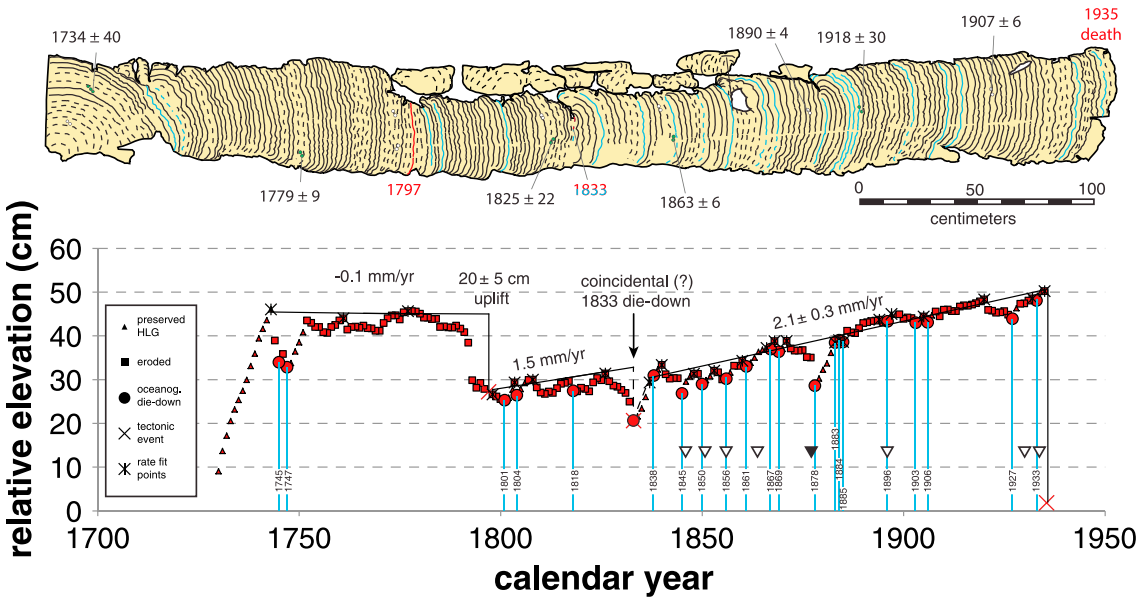

Figure 7. Cross section and growth history of BDG00-A1 from West Badgugu, which lived for more than 200 years. Symbols as in Figure 5. Blue lines mark die-down years; triangles mark moderate (empty) and strong (filled) IOD events between 1845 and 1935 from *Abram et al.* [2008]. Most IOD events are potentially correlated with die-downs, and the strong 1877 IOD is correlated with a particularly large die-down. The 1861 die-down may be an effect of the Nias-Simeulue megathrust earthquake in that year rather than an oceanographic event. This coral records a 20 cm coseismic uplift in 1797 and a 5–10 cm recovered die-down in 1833; however, the 1833 event may have been purely oceanographic. Interseismic deformation rates were low throughout the lifetime of this coral colony. Subsidence rates appear to have increased following the 1797 earthquake and possibly increased further after the 1833 earthquake, but due to uncertainties we cannot exclude the possibility of constant ~2 mm/yr subsidence for the full 200 years.

and Sikici D on Sipora, North North Pagai (an uninhabited, nameless bay), Basua on South Pagai, and the small islands of Pecah Belah, Simaturugogo, and Simungguk in the archipelago southeast of South Pagai (Figure 3). We also collected slabs from living microatolls at two other sites: Pulau Karangmadjat in the archipelago south of Siberut, and Pulau Simasin off the north coast of Siberut. The Karangmadjat modern subsidence rate is only 3.9 mm/yr, considerably lower than other sites at the southwest end of Siberut. The Simasin record is flat with essentially zero deformation, suggesting that it lies on the hinge line of interseismic deformation. Complete descriptions of all of these sites and slabs are in the supporting information Figures S4–S18.

We complete our data set with slabs from six additional new sites: Pulau Panjang C and North Pukarayat on Sipora, Pasapuat and Silabusabeu on North Pagai, a second site on the Pecah Belah islet, and a new site on Sanding, a small island 30 km southeast of South Pagai (Figure 3). All of these sites have significant populations of microatolls which date to the seventeenth century or earlier, so they will be fully presented in a future paper discussing earlier Mentawai rupture sequences. Cross sections and growth histories of the relevant eighteenth- and nineteenth-century microatolls from these sites appear in the supporting information Figures S19–S24.

3.3. Patterns of Coseismic and Interseismic Deformation

Having produced these data sets with consistent methods, we are now in a position to compare patterns of interseismic and coseismic deformation in different time periods. At this juncture, however, it is necessary to consider the possible impacts of sea-level change over decades or centuries, so that we do not mistakenly ascribe climatic changes to tectonic processes.

3.3.1. Effects of Sea-Level Change

It is reasonable to assume that any climate-related changes in sea level would be regional in extent, affecting all Mentawai corals equally. This assumption is supported by satellite altimetry data covering the last few decades, which indicates that sea level across the Mentawai region has been rising uniformly by about 3.5 mm/yr [*Beckley et al.*, 2007]. If the modern period is representative of earlier periods, then spatial variations in rate within a given time period can only be explained tectonically. However, variations in rate from one time period to another may be due in part to differing rates of sea-level change.

It is known from tide gauge records that during the twentieth century, the globally averaged rate of sea-level rise was ~1.7 mm/yr [*Church and White*, 2006]. Due to changing wind and ocean circulation patterns, sea-level trends in individual ocean basins differed significantly from this average, ranging from 0 to 5 mm/yr [*Church et al.*, 2004]. Unfortunately, there are few data constraining twentieth-century sea-level change in the Indian Ocean. A reconstruction by *Church et al.* [2006] based on long-term tide gauge records and recent satellite altimetry suggests a very high rate of sea-level rise (4 mm/yr) southwest of Sumatra. However, the accuracy of this result is questionable since their model includes only one long-term tide gauge in the Indian Ocean, located across the ocean from Sumatra. *Jevrejeva et al.* [2006] used a different tide gauge data set and methodology to estimate basin-wide trends. Their results suggest that the average rate of sea-level rise over the twentieth century in the Indian Ocean has been similar to the global average but fluctuated significantly: increasing from 2 mm/yr in 1910 to 4 mm/yr in 1940, then steadily decreasing to less than 1 mm/yr in 2000. However, their tide gauge data set also does not include any records from Sumatra [*Woodworth and Player*, 2003].

Rates and patterns of sea-level change in the 18th and 19th centuries are of course even less well known. Few if any tide gauge records extend so far back. While the effects of anthropogenic climate change were presumably smaller than in the twentieth century, other natural climate fluctuations (such as the Little Ice Age) undoubtedly contributed. Reconstructions of sea level around the world over the last 2000 years typically suggest rates of change less than 1 mm/yr [*Kemp et al.*, 2011], but these records do not preclude higher-magnitude fluctuations of sea level change on the scale of a century. A rise of 1 mm/yr sustained over a century would change sea level by only 10 cm, which could easily go unnoticed if sea level then fell during the next century.

Given the poor constraints on decade- and century-scale sea-level change in the Mentawai region, we elect to present our interpretations of interseismic deformation rates without correction for sea-level change. We note that we must be cautious in comparing the magnitudes of interseismic rates between different time periods, but we can be fairly confident that changes in deformation patterns within the spatial extent of our study area reflect tectonic processes rather than climatic processes. The most significant potential effect on our results is in the estimation of coseismic uplift in 1833, since this depends on the extrapolation of modern interseismic rates over ~160 years. For instance, correcting for the global average rate of sea-level rise would essentially uniformly reduce our calculated 1833 coseismic uplifts by 27 cm, and both the coseismic and interseismic hinge lines would be shifted southwest toward the islands. However, as with the interseismic measurements, the spatial patterns of coseismic uplift would be unaffected.

3.3.2. Changing Interseismic Deformation Patterns

Figure 8 shows contour maps of interseismic deformation rates for the decades prior to 1797, the decades between 1797 and 1833, and for the latter half of the twentieth century. The measurements of rates for each of these periods are independent of the measurements for the other two periods, as they are derived from relative elevations of growth bands on individual microatolls and do not depend on absolute elevation measurements. The first and last periods show generally similar patterns: southwestward tilt, expressed as an increasing gradient of subsidence rate from northeast to southwest across the islands, roughly perpendicular to the strike of the trench. The hinge line between uplift and subsidence is constrained by data only near the northern end of the maps, but by extrapolation is likely located 30–50 km northeast of Sipora and the Pagai Islands. Data from the Batu Islands illuminate the interseismic hinge line and a zone of uplift that lies above the downdip edge of the locked zone [*Sieh et al.*, 1999], but our coral records from this area are unfortunately limited to the late nineteenth and twentieth centuries.

One significant deviation from this southwestward tilt is apparent in the twentieth-century records: lower subsidence rates nearer to the trench south of Siberut and on the north end of Sipora define a peak in subsidence rates about 100 km from the trench. This pattern implies decreasing coupling trenchward of the islands. Unfortunately, our data do not constrain whether this was also the case in the pre-1797 period. However, both the twentieth-century and pre-1797 patterns are consistent with the updip limit of locking on the megathrust being beneath the southwest coasts of the islands. It is not surprising that deformation patterns in these two periods are similar, as they both cover the five decades or so leading up to the initiation of a supercycle rupture sequence.

In contrast, the deformation pattern during the period between the two great earthquakes is markedly different from the patterns observed during the modern period and before 1797. The data for this period

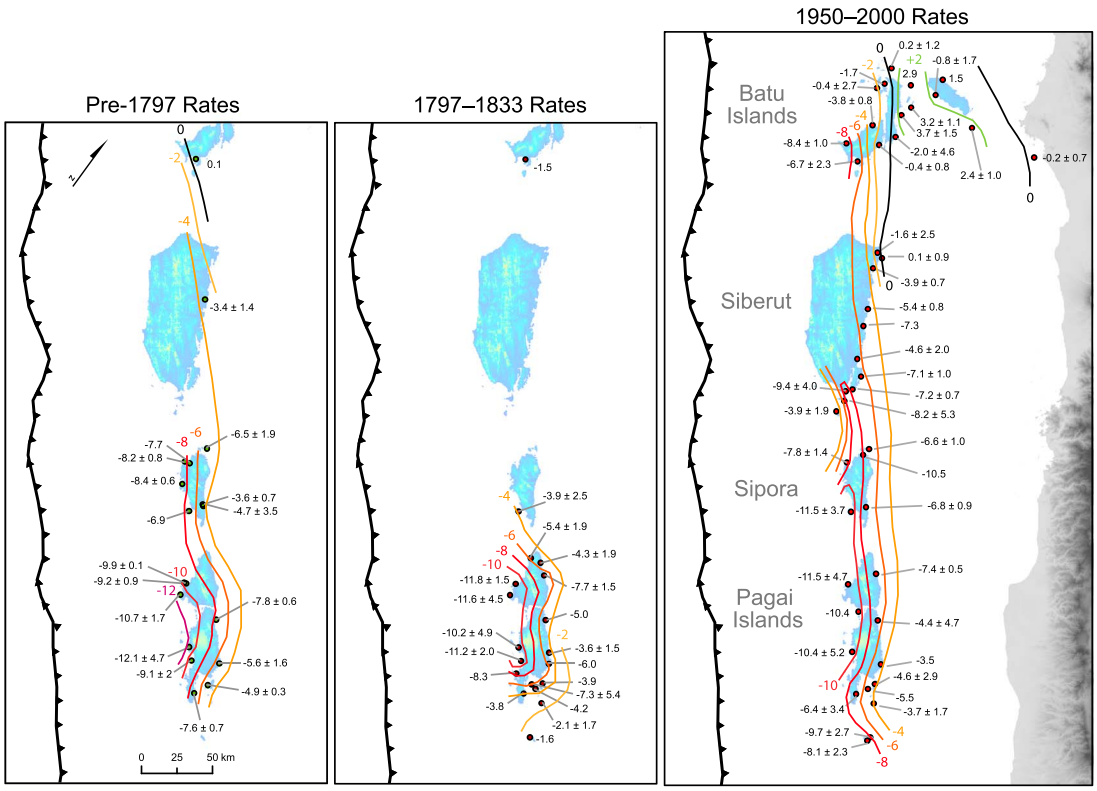

Figure 8. Patterns of interseismic subsidence during three temporal periods. All measurements are in mm/yr, contoured at 2 mm/yr intervals. Positive and negative numbers indicate uplift and subsidence, respectively. Uncertainties shown are 95% confidence intervals; measurements without uncertainties have too few fit points to calculate a meaningful uncertainty. The pre-1797 pattern is similar to the twentieth-century pattern, both of which cover time periods leading up to the beginning of a rupture sequence. However, the period between the two great earthquakes is marked by lower subsidence rates on Sipora and the southern end of South Pagai. It is not known how these patterns might have changed following the 1833 earthquake, as the reefs died completely due to uplift in that event and no corals from the later nineteenth century appear to have been preserved in the intertidal zone.

are more limited in spatial extent, but there were clearly steeply decreasing gradients in subsidence rate along strike from the southeast end and likely also the northwest end of the Pagai Islands. This suggests that the 1797 rupture reduced the degree of coupling on at least two separate patches of the megathrust. However, the magnitude and pattern of subsidence throughout most of the Pagai Islands remained similar to what it had been prior to the 1797 rupture. It is not known how coupling patterns might have changed following the 1833 earthquake, as the reefs died completely due to uplift during that event and no corals from the later nineteenth century appear to have been preserved in the intertidal zone. We can conclude only that by 1950, interseismic coupling patterns had returned to a more "normal" state. While it is now recognized that viscoelastic relaxation can affect deformation for decades after large earthquakes, these effects decay with time and are less prominent in the near field [*Wang et al.*, 2012], so it is unlikely that more than three decades of constant-rate deformation merely expresses a viscoelastic effect.

The notable change in deformation pattern after the 1797 earthquake, which was the beginning of a Mentawai rupture sequence, is intriguingly analogous to recent changes measured by the Sumatran GPS Array (SuGAr) following the 2007 Mentawai earthquakes. Seven years after the earthquake, interseismic deformation rates have still not returned to pre-2007 conditions and appear to have stabilized at lower rates rather than continuing the typical postseismic logarithmic decay, suggesting reduced coupling [*Qiu et al.*, 2012]. Based on the historical rupture sequence, we expect that this new coupling state will persist, perhaps for decades, until the next major rupture in the sequence occurs. This interearthquake coupling pattern will no doubt influence the slip distributions of future ruptures. Additional potential modern analogues may be found in the comparison of GPS velocity data sets before and after 2001, which suggest that coupling decreased in the Batu Islands and Enggano regions around that time [*Prawirodirdjo et al.*, 2010]. The sparse

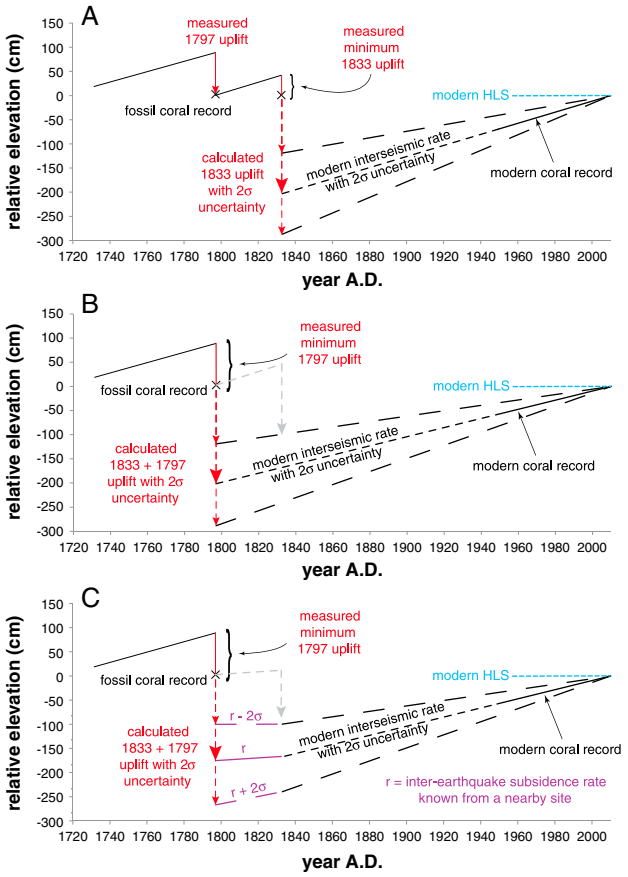

Figure 9. Calculations of total coseismic uplift in cases where (a) 1797 uplift can be measured directly; (b) all nearby reefs died completely in 1797; and (c) interearthquake subsidence rate (different from the modern rate) is known from a nearby site.

temporal sampling of campaign GPS data sets makes it unclear exactly when the changes occurred, but the 2000 Enggano earthquake and 2005 Nias-Simeulue earthquake are obvious candidates for the triggering of these coupling changes.

3.3.3. Coseismic Uplift Distributions

At many of our sites, coseismic uplift in 1797 is directly measureable on microatolls which survived that event. However, no microatolls that we have found (except for the Badgugu specimen) survived the 1833 uplift. As previously noted, all uplifts for 1833 are calculated by projecting the modern subsidence rates (with uncertainty) back to the time of the earthquake, and subtracting this assumed postearthquake elevation from the known preearthquake HLS. Figure 9 schematically illustrates how this is done, and Figure 10 shows the resultant uplift distributions for the great earthquakes of 1797 and 1833. For fossil coral sites where no modern coral was collected, we use rates from nearby sites or interpolated modern rates based on the twentieth-century contour map in Figure 8 (see Table 2).

At some sites (particularly on Siberut and Sipora), the intertidal fringing reefs died completely in 1797 and had apparently not reestablished themselves by 1833. At these sites, we add the additional subsidence between 1797 and 1833 to estimate the total coseismic uplift due to both earthquakes (black numbers in Figure 10). For sites on the Pagai Islands we use the known rates for 1797–1833 period (Figure 9c), but for those on Siberut and Sipora we assume that the rates between 1797 and 1833 were the same as the modern rates (Figure 9b), because our data do not constrain the interearthquake behavior there. If the subsidence between 1797 and 1833 was indeed slower than the modern subsidence at any of those sites, the total coseismic uplift we calculate is overestimated by as much as ~20 cm. Finally, we partition the uplift between the two earthquakes (parenthetical numbers in Figure 10) based on the trends of more certain contours and likely uplift gradients. The uplift distributions we infer are reasonable, given that the uplift gradients we derive are similar to those observed for the 2005 and 2007 coseismic uplifts [*Briggs et al.*, 2006; *Sieh et al.*, 2008].

It should be noted that none of our methods can distinguish between coseismic and postseismic uplift, as fossil microatolls are inevitably too eroded to distinguish uplift that occurred within a few years of the initial event from the sudden coseismic uplift. (Postseismic uplift can, however, sometimes be discerned in modern coral records such as PJG12-C5; see Figure S20). Thus, our "coseismic" uplifts probably represent summations of coseismic and postseismic uplift. However, in contrast to afterslip on the same patch which ruptured coseismically, postseismic slip surrounding the coseismic rupture area would produce postseismic vertical deformation opposite the coseismic deformation. Indeed, afterslip following the recent ruptures of the Sunda megathrust has generally followed this pattern [e.g., *Gunawan et al.*, 2014; *Hsu et al.*, 2006; *Lubis et al.*, 2013; *Paul et al.*, 2007, 2012], so it is likely that the ancient ruptures behaved similarly. Therefore, our coral records more likely include postseismic subsidence rather than postseismic uplift. Unless it occurred within a few days of the coseismic event, postseismic subsidence would not decrease the observed coseismic uplift,

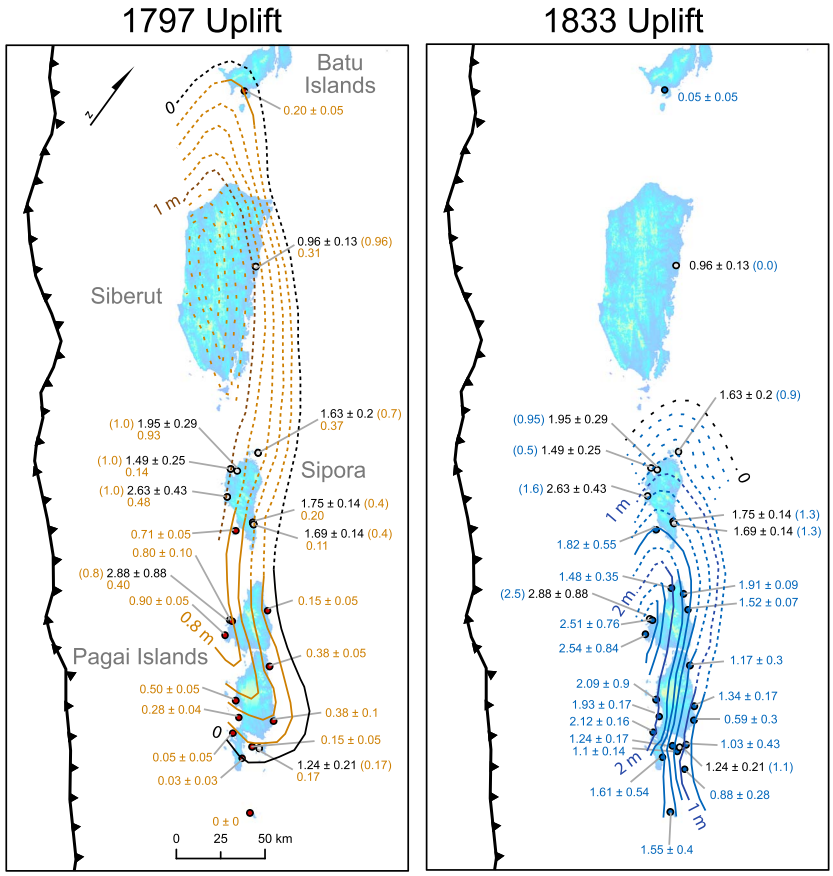

Figure 10. Coseismic uplift patterns of the great 1797 and 1833 earthquakes. Measurements are in meters and are contoured at 20 cm intervals. All uncertainties are 95% confidence intervals. Gray circles indicate sites where reefs died completely in 1797, so the partitioning of uplift between the two earthquakes is uncertain. At these sites, black numbers show totals and parenthetical colored numbers show inferred uplift for each earthquake. Minimum 1797 uplift at these sites is shown below black numbers on 1797 map. Dashed contours show inferred uplift at these sites based on likely uplift gradient and trends of more certain contours. Dotted contours are conjectural.

because the coral would still die before it was postseismically resubmerged. Unfortunately, postseismic subsidence is also difficult to discern in coral records because it is superimposed on interseismic subsidence and oceanographic fluctuations. Most of our coral records may include a few centimeters of postseismic subsidence; however, in most cases this subsidence is constrained to be a small percentage of the uplift, at most.

Our data clearly resolve the southeastward lessening of the 1797 uplift across the Pagai Islands and termination of uplift near the southern tip of South Pagai. The northwestern terminus is constrained by the Badgugu record, though less well. Though our one site on Siberut cannot constrain much of the uplift pattern, it is likely that 1797 uplift peaked on central or southwestern Siberut, as the uplift gradients trend toward that area from both ends.

For 1833, the trench-parallel pattern of contours over the Pagai Islands is largely derived from that same pattern in the modern interseismic rates, since the uplifts are estimated by projecting those rates. The southern terminus of the rupture was apparently well southeast of Sanding Island, as there is no hint of a southeastward decreasing uplift gradient between South Pagai and Sanding. However, northwestward decreasing uplifts between North Pagai and Sipora (and plausibly across Sipora) imply that the magnitude of slip on the underlying megathrust tapered off beneath those islands. Due to the death of fringing reefs in 1797, the precise northwestern extent of the 1833 uplift is not constrained, but extrapolating the established uplift gradient to the northwest yields a point of zero uplift south of Siberut. The growth of the Badgugu coral much farther north was apparently perturbed in 1833, but as previously discussed this is likely an oceanographic event coincidentally in the same year. There is no evidence of uplift in 1833 or 1797 on Nias Island farther north, and any significant amount of uplift is precluded by coral records [*Meltzner et al.*, 2014].

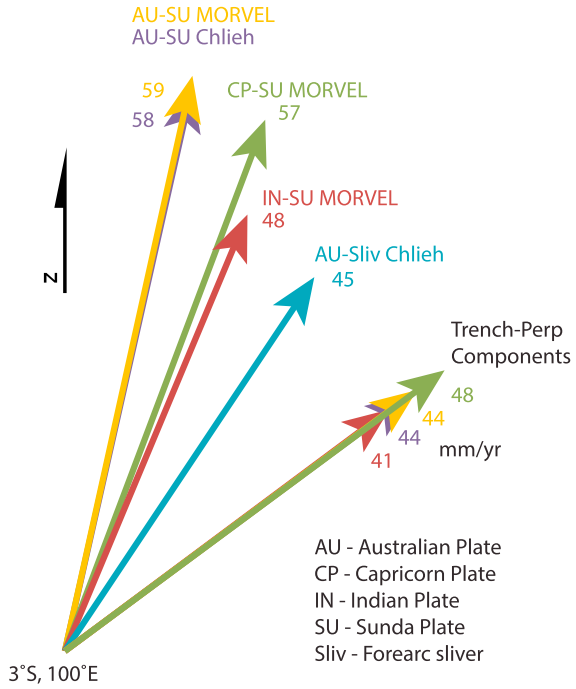

Figure 11. Comparison of relative plate motions in the Mentawai region according to the MORVEL-1 global model [*DeMets et al.*, 2010] and the regional GPS-based model [*Chlieh et al.*, 2008].

In summary, these coseismic uplift patterns are consistent with primary rupture patches downdip of the islands, though we cannot exclude the possibility that some parts of the shallow megathrust slipped as well (updip of Siberut for 1797 and updip of the Pagai Islands for 1833). The broad zone of overlap between the two uplift patches almost certainly indicates rerupture in 1833 of the southeastern and central portions of the 1797 rupture patch.

4. Modeling Megathrust Behavior

To estimate more quantitatively the underlying slip on the megathrust that is presumably the source of the surface deformation patterns we observe, we employ inverse modeling techniques. We assume that the medium surrounding the megathrust can be considered to be linear elastic, as is customary in modeling studies of coseismic and interseismic deformation [e.g., *Cohen*, 1999]. It is well established that this elastic dislocation theory typically works well for modeling coseismic deformation. Its application to interseismic deformation is more questionable because of possible deformation within the hanging wall or footwall of the megathrust, such as secondary faulting in the fore arc or bending of the subducting plate. However, in the case of the Sumatran Sunda megathrust the assumption of negligible long-term deformation of the hanging wall is supported by observations of low long-term deformation rates [*Briggs et al.*, 2008; *Philibosian et al.*, 2012]. To relate surface displacement to fault slip at depth, we use the analytical solutions of *Okada* [1992] which assume a homogenous linear elastic half-space, implemented as part of the Principal Component Analysis Inversion Method (PCAIM) code (see section 4.2). Because surface strain carries very little information about fault geometry at depth [e.g., *Vergne et al.*, 2001], the geometry of the megathrust must be described a priori. We model the megathrust as a curved fault plane made up of 15×15 km rectangular patches, starting at 1.2 km depth and 7.5° dip below the trench axis and ending at 100 km depth and 29° dip below the Sumatran coastline, a two-dimensional approximation of the Slab 1.0 model [*Hayes et al.*, 2012]. Our model places the flat free surface at the trench seafloor and ignores the ~6 km of topography between that datum and the islands. This simplification may result in underestimates of the fault slip required to produce the observed deformation, but the effects of topography on vertical elastic deformation are likely no more than a few percent [*Hsu et al.*, 2011].

The total relative tectonic motion in our study area is between 48 and 59 mm/yr, depending on whether a regional or global model is used and on whether the subducting plate is considered to be India, Australia, or Capricorn (Figure 11). The oblique convergence between the Indian/Australian and Sunda plates is a classic example of strain partitioning, with the convergence concentrated on the subduction zone and the lateral motion on the right-slip Sumatran fault [e.g., *Fitch*, 1972; *McCaffrey et al.*, 2000]. In reality, the subduction beneath the fore-arc sliver between the two fault traces is still slightly oblique, as originally observed by *McCaffrey et al.* [2000] and shown by the regional model of *Chlieh et al.* [2008] (Figure 11). However, for the purposes of our modeling, we ignore this small oblique component and restrict the megathrust to dip-slip motion because the measurement of vertical displacements alone cannot constrain the strike-parallel component of slip. This component is known to have been small for the coseismic slip during the recent large earthquakes in the area [*Konca et al.*, 2007, 2008] and for the recent period of interseismic strain [*Chlieh et al.*, 2008]. For our interseismic coupling models, we adopt the back slip modeling approach pioneered by *Savage* [1983], representing megathrust coupling as the mathematically equivalent backward slip on the fault interface. We define 100% coupling as back slip equaling the trench-perpendicular convergence across

Table 3. Reduced Chi-Square, Moment, and Moment Magnitude for Coseismic Models

	Pinned Below Trench			Free Below Trench		
Model	χ^2_r	M_0 (N m)	M_w	χ^2_r	M_0 (N m)	M_w
1797	0.75	1.2×10^{22}	8.65	0.65	2.1×10^{22}	8.82
1833	1.08	1.8×10^{22}	8.78	1.12	2.5×10^{22}	8.86
2007 (coral only)	1.32	1.2×10^{22}	8.67	1.28	2.4×10^{22}	8.85
2007 (coral + GPS)	0.99	1.3×10^{22}	8.67	0.96	1.5×10^{22}	8.71

the subduction zone, which is 41–48 mm/yr depending on which plate is used (Figure 11). We adopt the rate of 44 mm/yr based on the regional model of Australia-Sunda subduction [*Chlieh et al*., 2008], which translates to ~45 mm/yr slip on the dipping megathrust.

To relate slip on the megathrust to the seismic moment classically used to quantify earthquake sources, we follow *Chlieh et al*. [2008] by using a shear modulus of 65 GPa, based on the average (down to 100 km depth) of the one-dimensional CRUST 2.0 layered structure model for this region [*Bassin et al*., 2000]. While the regional layered structural model does not take subduction zones into account, increasing rigidity with depth is consistent with observed earthquake parameters, and 65 GPa is a likely average value for megathrust ruptures at depths of 40–60 km [*Bilek and Lay*, 1999; *Lay et al*., 2012].

As is typically the case for buried elastic dislocation models, inverting the observed surface deformation for slip at depth is a highly underconstrained problem. We regularize our solutions by penalizing rough slip distributions. In effect, we minimize a cost function CF that is the sum of the reduced chi-square error (the first term in the equation below) and the Laplacian of the slip distribution ($\nabla^2 S$):

$$\mathrm{CF} = \frac{1}{N-P}\sum_{i=1}^{N}\frac{o_i - p_i}{\sigma_i^2} + \lambda\nabla^2 S \tag{1}$$

Here N is the number of observations, P is the number of parameters being fit, σ_i is the uncertainty assigned to each observation o_i, and p_i is the corresponding model prediction. The Laplacian penalty λ, which quantifies the degree of smoothing from each patch to its neighboring patches, is weighted locally based on how precisely the data can resolve slip on that patch. Our implementation of this method, originally developed by *Lohman* [2004], is modified following *Ader et al*. [2012]. In essence, it applies a strong smoothing to poorly resolved areas of the fault plane far from our observations while permitting a rougher distribution of slip in areas directly beneath our observation sites. Resolution distributions for each of the models appear in the supporting information (Figures S29–S31 and S35). For each model, we apply the maximum weight to the Laplacian penalty (scale factor of λ) that provides misfits to the data of the order of the average data uncertainties (reduced chi-square of ~1; see Figure S26). For each model presented below we report the value of the reduced chi-square in Tables 3 and 4.

Inverting for fault slip based on coral data has an additional limitation over using Global Positioning System (GPS) data, since coral provides only the vertical component of deformation. As noted above, we restrict our models to pure dip slip for this reason. To illustrate that coral data do capture the important features of underlying fault slip, we produced a test model of the combined slip during the September 2007 earthquakes using coral data only and compared this to a model using both coral and GPS data (Figures S27–S29). The two models have almost equal magnitudes of 8.67 and both reproduce the dumbbell shape noted by *Konca et al*. [2008]. Our magnitudes are somewhat larger than the 8.5 estimated by *Konca et al*.,

Table 4. Reduced Chi-Square and Moment Deficit Rate for Interseismic Models

	Uncoupled Below Trench		Free Below Trench	
Model	χ^2_r	M_0/yr	χ^2_r	M_0/yr
1755–1795	0.78	7.5×10^{19}	0.70	1.0×10^{20}
1798–1832	0.78	6.1×10^{19}	0.70	7.4×10^{19}
1950–2000 (coral only)	1.10	1.6×10^{20}	1.19	2.6×10^{20}
1950–2000 (coral + GPS)	1.73	3.3×10^{20}	1.69	3.6×10^{20}

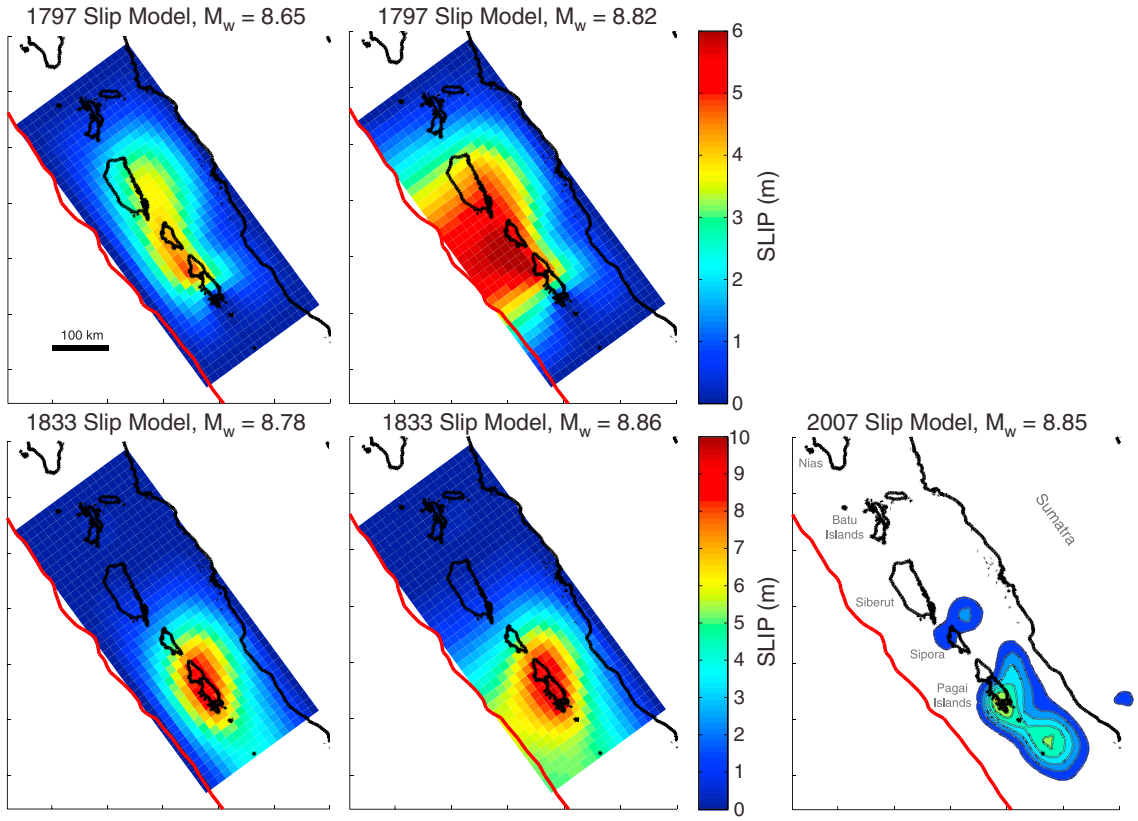

Figure 12. Slip models of the 1797 and 1833 earthquakes based on coral uplift data (note differing color scales). Left column shows end-members with no slip permitted at the trench, while models in the right column are permitted to slip at the trench. Due to the lack of resolution far from the islands, both types of models can fit the data equally well. For comparison, the total 2007 coseismic slip contoured at 1 m intervals (starting at 1 m), from *Konca et al.* [2008], is shown using the same color scale as for 1833.

likely due to our curved fault surface (which plunges much more deeply beneath the Sumatran coast) and to differences in smoothing. Based on this test, there is good reason to believe that inversions based on coral data alone are reliable to first order.

4.1. Coseismic Slip Models

Figure 12 shows possible coseismic slip models for the two great earthquakes. All models are forced to zero slip at the base of the fault (100 km depth) as this is likely the base of the seismogenic zone, and no significant slip at this depth has been observed during the modern large megathrust earthquakes either in Sumatra or elsewhere. Models for 1797 are not permitted to slip along the northwest or southeast edges of the fault, as our data suggest the slip terminated within the bounds of our fault patch. Models for 1833 are permitted to slip along the southeast edge, as there is no reason to believe the rupture did not extend in that direction beyond our data. For each earthquake, we present two slip distributions: one for which slip is forced to zero below the trench, and one for which slip is not constrained below the trench. In the latter case, the penalty on the Laplacian favors large slip updip of the Mentawai Islands because the data themselves do not express any significant updip tapering of slip, so the slip gradient below the islands is extrapolated updip. As deformation measurements on the Mentawai Islands are not sensitive to slip near the trench, both classes of models can fit our coral uplift data equally well, and the differences in residuals are nearly imperceptible (residuals are shown in Figure S30). These models can be considered as end-members, bracketing the 1797 earthquake between moment magnitudes 8.6 and 8.8 and the 1833 earthquake between 8.8 and 8.9. Misfits, moments, and moment magnitudes are summarized in Table 3.

The higher-slip end-members could be considered "Tohoku 2011-type" events, with large areas of slip concentrated on the shallow part of the megathrust, and could produce similarly devastating tsunamis.

The end-members with slip limited to intermediate depths would produce minor tsunamis similar to the 2007 main event [*Borrero et al*., 2009]. Given the major tsunamis reported at Padang in 1797 and Bengkulu in 1833 (from historical records summarized by *Natawidjaja et al*. [2006]), some slip likely extended to the shallow megathrust during both events, though not necessarily as much as in our end-member models. Based on the assumed fault slip rate of 4.5 cm/yr, the ~6 m of maximum modeled slip in 1797 would build up after only 130 years (assuming a complete locking of the plate interface during the interseismic period), while the larger ~10 m slip in 1833 would require 220 years, comparable to the Mentawai supercycle recurrence interval estimated by *Sieh et al*. [2008].

Our models are generally similar to the simpler forward models made by *Natawidjaja et al*. [2006] but are better constrained and more realistic since they lack the artificial abrupt transitions in slip magnitude. Our adjustments and additions to the data set removed some features that had been very difficult to fit (such as an extremely abrupt termination of uplift at the southern end of the 1797 rupture). Our models confirm that the 2007 Mentawai ruptures, which collectively released a moment of about 7.5×10^{21} Nm (equivalent to a M_w 8.5 earthquake), were in total significantly smaller than the 1833 rupture, as noted by *Konca et al*. [2008] and *Sieh et al*. [2008]. Slip in 2007 (shown for comparison in Figure 12) approximately equaled our lower end-member model of 1833 slip in the area between Sanding and Mega islands but was about 50% less beneath South Pagai and nonexistent beneath North Pagai and southern Sipora.

4.2. Interseismic Coupling Models for the Eighteenth and Nineteenth Centuries

To model interseismic coupling, we employ the Principal Component Analysis Inversion Method (PCAIM) developed by *Kositsky and Avouac* [2010] using the iterative decomposition method described by *Perfettini and Avouac* [2014]. PCAIM performs a singular value decomposition of the time series data matrix, $d = USV^t$, where S is a diagonal matrix of eigenvalues, the vectors U and V represent the spatial distributions and time functions associated with each component, and ^{t} indicates the matrix transpose. Components are ordered according to their respective contribution to explaining the data variance. The data are then filtered by discarding the lower-order components, since the primary features of the data can be reproduced by the first few components. PCAIM then inverts the spatial deformation field (U) components to obtain fault slip components (L), and recombines V with L to produce a complete time series of slip on the fault plane. This method greatly reduces the otherwise very large number of computations necessary to model a deformation time series and allows the combination of time series with different observation epochs and variable uncertainties. Also, with the decomposition being performed on the entire data set (rather than considering time intervals as has been classically done), greater consistency is expected. Table 4 summarizes model misfits and moment deficit rates for all our interseismic models.

To prepare the coral time series for modeling, we assign uncertainties of ±2.6 cm to die-down and HLG points, ±5–10 cm to moderately eroded points, and remove severely eroded points. The uncertainty for uneroded points is based on the natural variability in coral HLS [*Natawidjaja et al*., 2004] and is increased based on the estimated amount of erosion for eroded points. We do not include any HLG points before a coral first reached HLS, since such points were not limited by relative sea level. We use a single time series for each site (either from the single longest, best-preserved sampled coral or a concatenation of coral records covering different time periods) and remove the 1797 coseismic uplift. To minimize differences between the models which could be spuriously induced by differing spatial distributions of data, we also include a synthetic data set based on a model of all the coral data (ancient and modern) with a linear time function. To create the synthetic data set, we add uncertainties of ±10 mm/yr to the predictions of the all-coral model and include this synthetic data for each location that has no real data within the model's time period. Thus, the distribution of sites and resultant spatial model resolution is the same for all coral-based interseismic models (see Figure S31). We also augment the real data by extrapolating each time series to fill the entire model time period, using the synthetic rates and uncertainties derived above.

A four-component model provides the best fit to the 1755–1833 interseismic deformation (Figure 13). As the first-order signal is clearly linear, we impose a linear time function as the first component so that deviations from linear are more clearly shown in subsequent components. The second component accounts for the major oceanographic die-down in 1776 and is removed from the inversion. Other die-downs were insufficiently coherent to be modeled as individual components. These remain in the

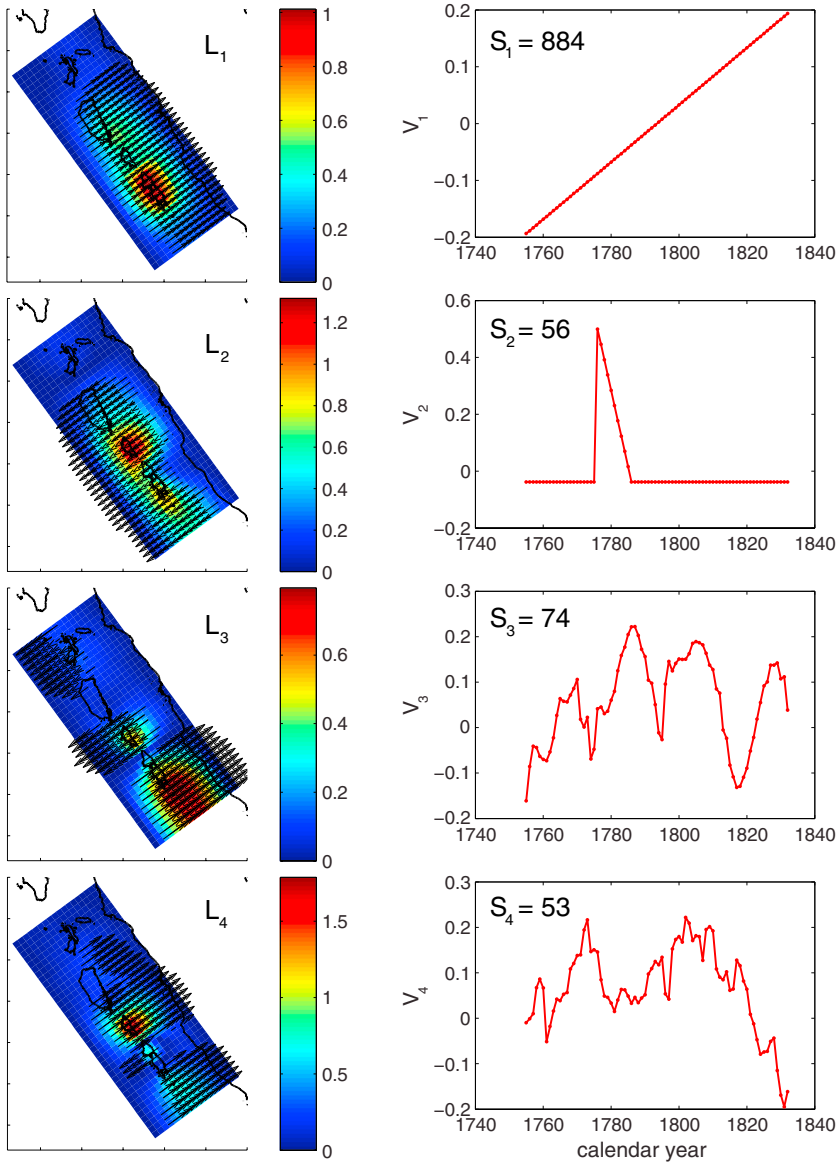

Figure 13. Spatial (*L*) and temporal (*V*) eigenvectors for the four-component 1755–1833 interseismic deformation model. Eigenvectors are normalized; eigenvalues (*S*) indicate the relative magnitudes of the components.

data and are modeled as megathrust slip, but since these are relatively small deviations that are typically recovered within a few years, this nontectonic contamination has little effect on the long-term average coupling we derive. The third and fourth components are unconstrained (adding further free components did not improve the fit to the data). Though somewhat obscured by oceanographic fluctuations, the time functions of the free components both change slope around the year 1797: V_3 slopes positively before and negatively afterward, and V_4 is approximately level before and plunges steeply negative afterward. The spatial eigenvectors L_3 and L_4 indicate that these changes are associated with patches beneath Sipora and southeast of South Pagai. Data and modeled time series (Figure S32) illustrate that this model provides a good fit at all sites.

Figure 14 illustrates that before the 1797 earthquake, there was a strongly coupled patch beneath the Pagai Islands and moderately coupled patches extending northwest and southeast. After 1797, the Pagai patch remained strongly coupled but the patches below Sipora and Sanding became nearly uncoupled. Coupling beneath Siberut is unconstrained after 1797. As with the coseismic cases, models where coupling of the

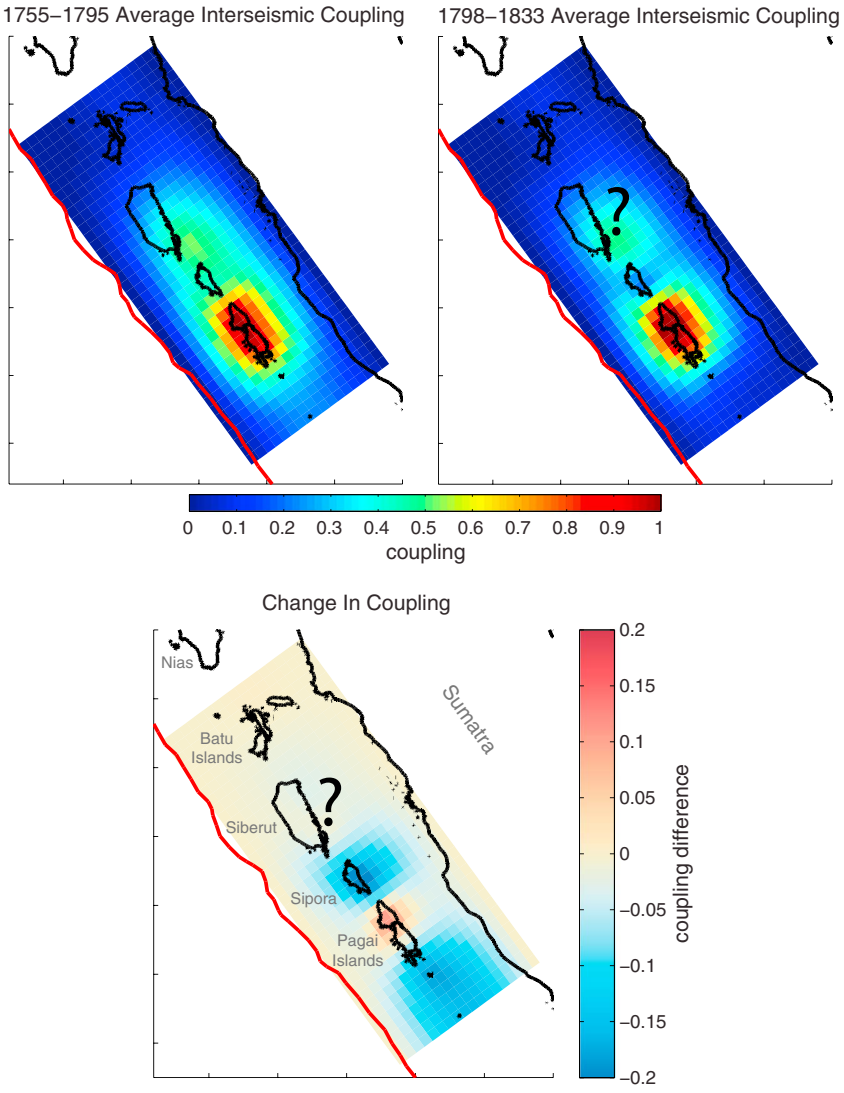

Figure 14. Megathrust coupling before and after the 1797 earthquake. Coupling beneath Siberut is not resolved after 1797 but substantially decreased coupling beneath Sipora and southeast of South Pagai can be seen clearly, while coupling increased slightly beneath the Pagai islands.

shallow megathrust is permitted can fit the data equally well (these alternate end-members are shown in Figure S37). Shallow coupling would of course be necessary to build up strain for coseismic events involving shallow slip, such as the 2010 [*Hill et al*., 2012] and circa 1314 [*Philibosian et al*., 2012] events.

4.3. Interseismic Coupling Models for the Twentieth Century

The previous inversions are based on vertical displacements only. For the modern period we have the opportunity to add horizontal displacements measured by GPS. It is therefore possible, for the modern time period, to compare models obtained from both the GPS and coral and from the coral data alone, unlike those presented for the 1755–1832 time period. We supplement the purely vertical coral data covering the 1950–2000 time period with horizontal campaign GPS data collected over 1991–2001 [*Bock et al*., 2003]. We calculate the motion of these stations relative to the fore-arc sliver using the Euler poles derived by *Chlieh et al*. [2008] and extract the trench-perpendicular component. While a small part of the trench-parallel motion of these stations is due to the slightly oblique subduction, most of the lateral motion can be attributed to strain accumulation across the locked Sumatran fault, and for our fixed-rake slip models it is more consistent to assume purely trench-perpendicular subduction. A similar approach has been used in other slip-partitioned subduction zones [*Feng et al*., 2012].

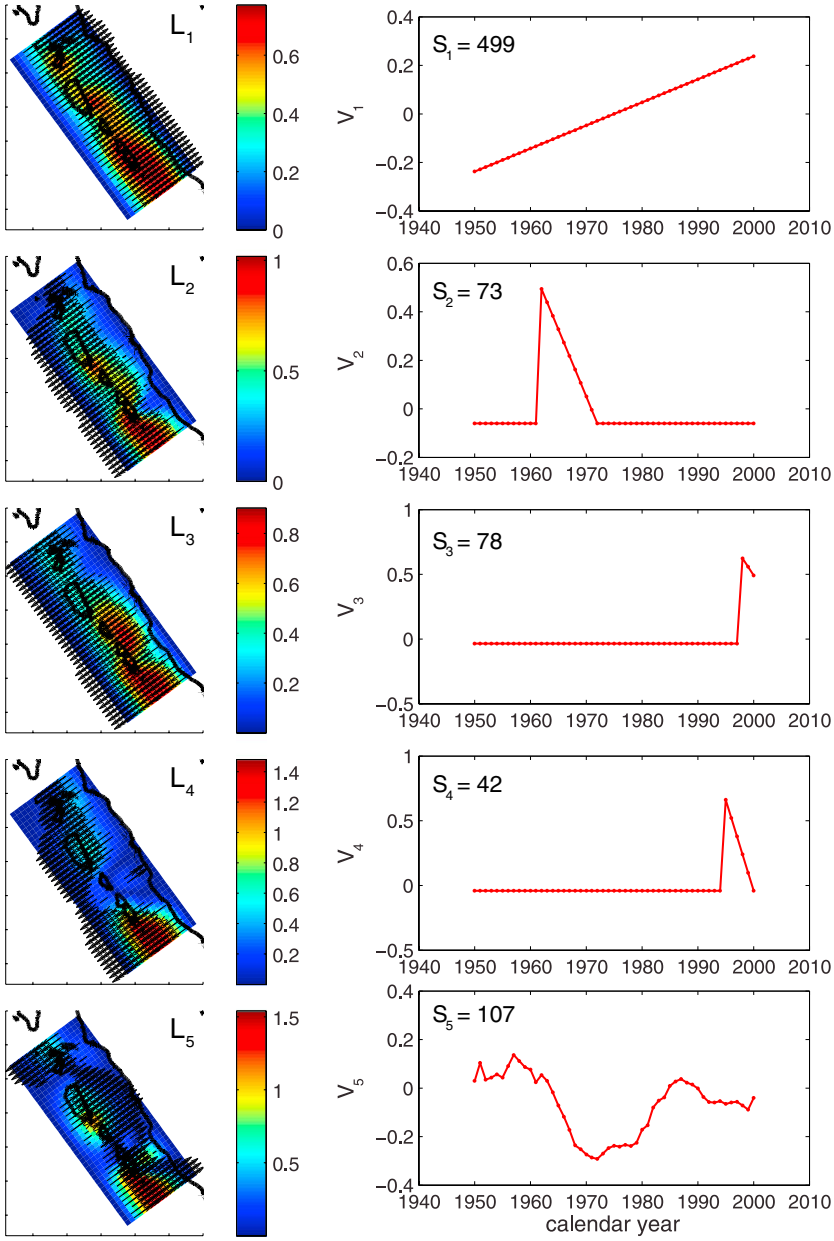

Figure 15. Spatial (*L*) and temporal (*V*) eigenvectors for the five-component 1950–2000 interseismic deformation model using only coral data. Components 2–4 are oceanographic.

Unlike *Chlieh et al*. [2008], we do not use any continuous data from the SuGAr network, as these stations were installed after the end of most of our coral time series. Furthermore, the SuGAr time series include many coseismic and postseismic events which make it difficult to discern the interseismic signal, and the postearthquake coupling state is likely significantly different from the preearthquake state represented by the twentieth-century coral time series (as we discovered was the case for the pre- and post-1797 periods).

We represent the modern interseismic period with a five-component model (Figure 15). As before, the first component has an imposed linear time function. Three of the oceanographic die-downs (1962, 1995, and 1998) are sufficiently coherent to be modeled with imposed components 2 through 4, which are removed from the inversion. The fifth component is unconstrained (adding further components did not improve the fit to the data). The fluctuation in V_5 appears to be primarily related to less coherent oceanographic events in the 1970s and 1980s, with no evidence for major changes in coupling.

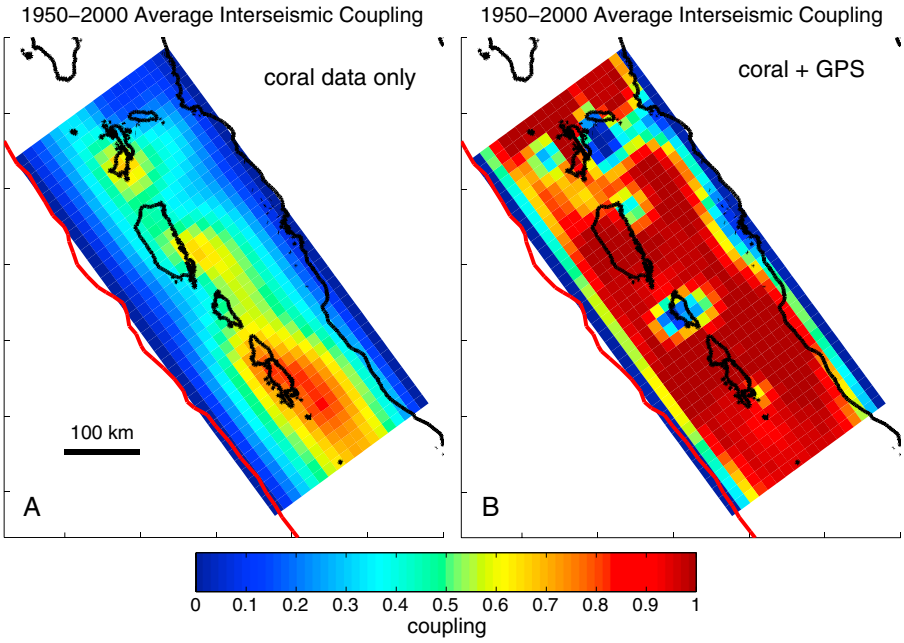

Figure 16. (a and b) Models of late twentieth-century megathrust coupling, based on coral and campaign GPS data. The GPS data require a much larger percentage of the fault plane to be fully locked than the coral data set alone does.

However, the fifth component is included in the inversion since some part of it may reflect tectonic processes. This model reproduces the time series of all sites well (Figure S33). The inversion (Figure 16a) produces a strongly coupled patch beneath the Pagai Islands and moderate coupling extending northwestward, fairly similar to the pre-1797 coupling pattern. Coupling was greater below the Batu Islands in the late twentieth century (as evidenced by the dramatically increased subsidence at Badgugu after the 1935 earthquake).

We then added the GPS data as a constraint on the inversion (but did not use them in the principal component analysis because they are too sparse in time to help constrain the time evolution). The five time functions are unchanged from the coral-only model, but the inverted spatial eigenvectors are significantly different (Figure S34). Figure 16b shows the resulting model which fits the GPS data quite well (residuals are shown in Figure S35) and the coral data reasonably well (Figure S36). The inclusion of the GPS data requires the majority of the fault to be completely locked, producing a coupling pattern unsurprisingly similar to the models of *Chlieh et al*. [2008], since most of the data and assumptions are the same. Our model has slightly increased coupling relative to *Chlieh et al*., likely due to our deeper curved fault surface and smoothing differences, as was the case with the comparison to *Konca et al*. [2008].

It is unclear whether the dramatic difference between the models with and without the GPS data occurs because the 10 year GPS measurement period was not representative of the 50 year period covered by the coral data, or because the GPS measurements are sensitive to coupling on areas of the fault that the coral measurements cannot resolve. As our experiment with the 2007 coseismic data illustrated, the coral data are not typically so insensitive to slip on large areas of the megathrust. Any adjustment for rising sea level to the coral-derived rates would only exacerbate the mismatch between the data sets.

5. Discussion

Comparisons between the modeled distributions of coseismic slip and interseismic coupling illustrate a number of interesting relationships. Of the two patches with decreased coupling after 1797, the northwestern one had ruptured in 1797 but the southeastern one was adjacent to the southern terminus of the rupture. The 1833 event then reruptured the southeastern half of the 1797 rupture, including both patches with reduced coupling. It is somewhat surprising that the 1833 rupture was able to propagate through both reduced-coupling patches, but perhaps the asperity beneath the Pagai Islands, which apparently became even more

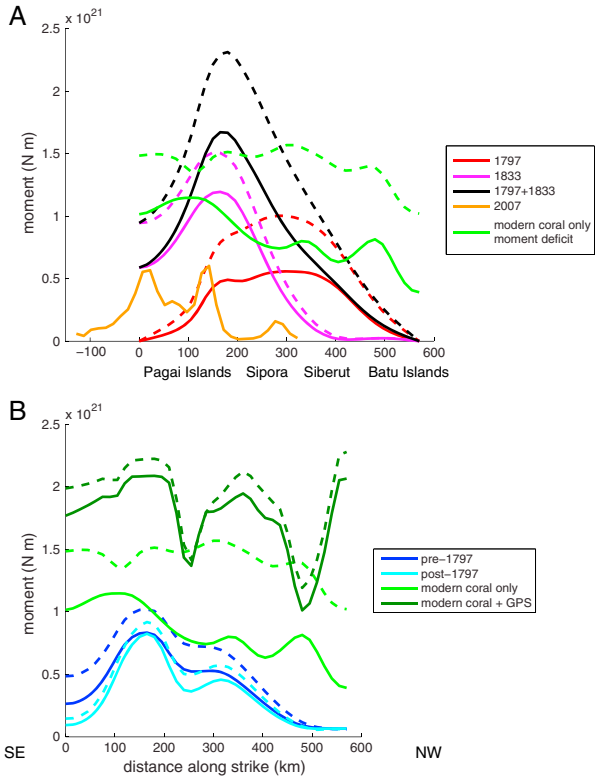

Figure 17. Comparison of seismic moment and moment deficits for our models, integrated over the 15 km model patch width. Solid and dashed lines indicate end-members with constrained and free updip edge of the fault, respectively. All interseismic deficits are for 210 years, the interval between 1797 and 2007. (a) Comparison of coseismic moments with the moment deficit of the modern coral-only model for reference. Moment distribution of 2007 earthquakes is from *Konca et al.* [2008]. (b) Comparison of moment deficits derived from all interseismic models.

strongly locked after 1797, facilitated the 1833 rupture propagation. The Pagai Islands asperity is a common feature of all our models, as the area with largest slip in 1833 and as a zone of strong coupling during every interseismic period, suggesting velocity-weakening friction with rapid healing of the fault interface after a rupture. The strain on this patch was clearly only partially released in 1797, since the 1833 slip is far too great to have accumulated in only 36 years.

The behavior of other areas is more variable, but it is clear that there must be multiple individual asperities on the megathrust. The patches beneath Sipora and Sanding have similar features in that both were moderately coupled prior to 1797, both became significantly less coupled afterward, and each formed a terminus of one of the two great earthquakes. Perhaps these areas of the megathrust exhibit velocity-strengthening friction and do not heal quickly after a rupture. In the twentieth century the Sipora patch was also moderately coupled, though the Sanding patch was apparently more strongly coupled. The paucity of data from Siberut prior to the twentieth century unfortunately leaves us unable to characterize the longer-term behavior of the megathrust beneath Siberut, but we can conclude that spatial variations in frictional properties on the megathrust beneath the Pagai Islands and Sipora potentially explain its distinctive characteristics: forming termini and major overlap of large megathrust ruptures and changing coupling after a large rupture. Model faults with heterogeneous frictional properties can reproduce the observed types of behavior [*Kaneko et al.*, 2010].

We can gain additional insight by comparing the along-strike moment distributions of the great earthquakes with moment deficits based on the various interseismic models (Figure 17). We use the moment deficit rate derived from the modern coral-only model as a reference. We apply this rate over 210 years, the interval between 1797 and 2007, and plot the variation along strike. The accrued moment deficit clearly exceeds the 1797 moment. Therefore, if that rate truly persisted over the entire interseismic period, sufficient moment potential for a repeat of the 1797 rupture has certainly accrued. This is the likely explanation for the difficulty of finding fossil microatolls from the eighteenth and nineteenth centuries on Siberut: the interseismic subsidence has so far exceeded the 1797 uplift that microatolls from that period now lie below the intertidal zone. Indeed, the lone 1797 microatoll field that we have found, at Silogui, lay ~15 cm below modern HLS when it was sampled in 2002 [*Natawidjaja et al.*, 2006], by far the lowest of all eighteenth- and nineteenth-century microatolls we have found, and has undoubtedly sunk even further in the decade since. Beneath the Pagai Islands and Sipora, the combined 1797/1833 moment exceeds the postulated moment deficit, perhaps explaining why slip tapered off in that area during the 2007 earthquakes.

A comparison of all the interseismic moment deficit rates, similarly converted to 210 year deficits (Figure 17b) illustrates that those derived from coral data alone are systematically lesser than those derived from a combination of coral and GPS data. If the coral records truly are insensitive to an important area of megathrust coupling, the moment deficit rates we derive for the 1755–1832 period, necessarily based on coral data alone,

are underestimated. Additionally, if the modern moment deficit rate derived from coral and GPS data is more accurate, the accumulated moment deficit exceeds the combined 1797/1833 moment nearly everywhere, and the potential for future earthquakes is significantly greater.

6. Conclusions

Our detailed analysis of the eighteenth-to-nineteenth century supercycle and comparison to the modern supercycle illustrate that major Mentawai megathrust ruptures are capable of altering fault coupling and likely influence how the rupture sequence proceeds, though the fault eventually returns to a "normal" interseismic coupling state before the next rupture sequence begins. Spatially and even temporally varying frictional properties of the megathrust beneath the southern Mentawai Islands likely prevent end-to-end ruptures of the Mentawai segment, producing the characteristic supercycle behavior. In terms of future seismic potential of the Mentawai segment, there are no indications that the accumulated seismic moment deficit is lesser now than it was prior to 1797. Therefore, the modern rupture sequence will probably include a rupture similar to the 1797 rupture, though perhaps with more slip beneath the Pagai Islands to make up for the difference between the 2007 and 1833 earthquakes. The tsunami hazard to the Mentawai islands and the adjacent Sumatran coastline remains high. The coupling variability we observe during the penultimate failure sequence implies that analysis of modern geodetic measurements may detect similar complexities prior to failure of the remaining locked parts of the Mentawai megathrust segment.

As microatoll-based studies of the Sunda megathrust provide one of the only records of multiple seismic cycles at high temporal and spatial resolution, it is instructive to compare this case to other major faults around the world. Our study highlights two major aspects of fault behavior: fault segmentation and variability of interseismic deformation. The Sumatran subduction zone presents examples of two distinct types of segmentation. Seemingly permanent barriers exist where large ruptures on both sides consistently have little or no overlap, as represented by the Batu Islands (discussed above) and Simeulue Island [*Meltzner et al*., 2012]. Areas with variable behavior, which sometimes act as barriers but where significant overlap of large ruptures also occurs, are exemplified by the middle of the Mentawai segment. As segmentation is a key control on maximum earthquake magnitude, mapping segmentation is one of the most important endeavors in the study of any major fault, and researchers have often attempted to divide faults into well-defined segments that rupture from end to end in characteristic earthquakes. However, it has become increasingly clear that persistent barriers to rupture are relatively rare on mature faults, and faults are more accurately described as being mosaicked by asperities which may rupture individually or in chains. Paleoseismic and historic earthquake chronologies for the South American [*Bilek*, 2010], Cascadia [*Goldfinger et al*., 2012], and Nankai [*Ando*, 1975] subduction margins all exhibit this type of behavior, and it is likely universal. Similar patterns have also emerged on continental faults [e.g., *Jewell and Bruhn*, 2013]. Observations of spatial heterogeneity in interseismic coupling also support the existence of "asperity mosaics" at the ~100 km scale in well-studied subduction zones such as Alaska [*Zweck et al*., 2002] and Japan [*Loveless and Meade*, 2010].

The Mentawai case is somewhat distinct from simple asperity mosaicking due to the large overlap zone between ruptures closely spaced in time. However, as more detailed studies are done and the nuances of fault behavior are revealed, there are hints that Mentawai-style behavior may not be so uncommon—the Mentawai case is perhaps merely the best-studied case. For example, along the south-central Chilean subduction margin, the Arauco Peninsula has been identified as a persistent boundary between the Concepción and Valdivia segments over several seismic cycles [*Melnick et al*., 2009], yet the 1960 Valdivia and 2010 Maule megathrust ruptures overlapped in that region by ~150 km [*Moreno et al*., 2011]. The 1960/2010 overlap zone is similar in size to the 1797/1833 overlap, though it represents a much smaller percentage of the total rupture area of the Chilean earthquakes. Records are not sufficiently precise to determine whether earlier Concepción and Valdivia ruptures overlapped or not [*Kelleher*, 1972], but large earthquakes on the two segments and on the Valparaiso segment to the north have frequently been tightly correlated in time [*Melnick et al*., 2009], which certainly qualifies as supercycle behavior, *sensu stricto*. Analogs to the Mentawai case are also not limited to subduction megathrusts; one potential continental example is the region linking the Mojave and Coachella Valley sections of the San Andreas Fault in California. Based on paleoseismic observations, many ruptures seem to terminate in this region [e.g., *Philibosian et al*., 2011; *Weldon et al*., 2004] and there was also significant overlap between the historical 1812 and 1857 earthquake ruptures [*Jacoby et al*., 1988].

Persistent, decades-long variations in fault coupling during the interseismic period have not been commonly identified, but this too may represent a lack of sufficiently detailed data rather than true rarity. Interseismic rate changes on the Nias-Simeulue segment have been identified based on coral records [*Meltzner et al.*, 2014], but such variations are difficult to discern with other paleogeodetic techniques, and the instrumental period is too short to encompass a significant percentage of the seismic cycle. We expect that as the instrumental geodetic period lengthens and more detailed paleogeodetic studies are made, more examples will emerge. Heterogeneities in fault frictional properties at the scale seen in the Mentawai case are probably common and control the rupture extent, magnitude, and distribution of slip in great earthquakes worldwide. The Mentawai example highlights many of the complexities researchers should expect to discover in seismic cycles on major faults around the world.

Acknowledgments

All data used in this paper are included in the main text or supporting information. This project was supported by the National Science Foundation grants 0208508, 0530899, 0538333, and 0809223 to K. S.; by the Sumatran Paleoseismology grant M58B50074.706022; by the National Research Foundation Singapore and the Singapore Ministry of Education under the Research Centres of Excellence initiative through the Earth Observatory of Singapore; by the Research Center for Geotechnology at the Indonesian Institute of Sciences (LIPI); by the Caltech Tectonics Observatory; and by the Gordon and Betty Moore Foundation. Also, the Japanese documentary agency NHK funded a special one- week final field expedition in 2012. U-Th dating was supported by the Taiwan ROC MOST and NTU grants 101-2116-M-002-009, 102-2116-M-002-016, 103-2119-M-002-022, and 101R7625 to C.-C. S. We thank Dudi Prayudi, Imam Suprihanto, John Galetzka, and all the crew members of the *K.M. Andalas* for field support, Ke (Coco) Lin for assistance with U-Th dating at the HISPEC Laboratory at the National Taiwan University, and Aron Meltzner, Emma Hill, Ashar M. Lubis, Lujia Feng, Louisa Tsang, Qiang Qiu, Joann Stock, Mark Simons, Paul Asimow, Marion Thomas, Thomas Ader, Andrew Kositsky, Kelly Wiseman, and Jeff Genrich for helpful discussions. This manuscript was improved thanks to reviews by Ya-Ju Hsu and an anonymous reviewer. This is Earth Observatory of Singapore contribution 70 and Caltech Tectonics Observatory contribution 259.

References

Abram, N. J., M. K. Gagan, M. T. McCulloch, J. Chappell, and W. S. Hantoro (2003), Coral reef death during the 1997 Indian Ocean Dipole linked to Indonesian wildfires, *Science*, *301*, 952–955.

Abram, N. J., M. K. Gagan, J. E. Cole, W. S. Hantoro, and M. Mudelsee (2008), Recent intensification of tropical climate variability in the Indian Ocean, *Nat. Geosci.*, *1*, 849–853.

Ader, T., et al. (2012), Convergence rate across the Nepal Himalaya and interseismic coupling on the Main Himalayan Thrust: Implications for seismic hazard, *J. Geophys. Res.*, *117*, B04403, doi:10.1029/2011JB009071.

Ando, M. (1975), Source mechanisms and tectonic significance of historical earthquakes along the Nankai Trough, *Tectonophysics*, *27*, 119–140.

Bassin, C., G. Laske, and G. Masters (2000), The current limits of resolution for surface wave tomography in North America, *Eos Trans. AGU*, *81*(48), Fall Meet. Suppl., Abstract S12A–03.

Beckley, B. D., F. G. Lemoine, S. B. Luthcke, R. D. Ray, and N. P. Zelensky (2007), A reassessment of global and regional mean sea level trends from TOPEX and Jason-1 altimetry based on revised reference frame and orbits, *Geophys. Res. Lett.*, *34*, L14608, doi:10.1029/2007GL030002.

Bilek, S. L. (2010), Seismicity along the South American subduction zone: Review of large earthquakes, tsunamis, and subduction zone complexity, *Tectonophysics*, *495*(1–2), 2–14.

Bilek, S. L., and T. Lay (1999), Rigidity variations with depth along interplate megathrust faults in subduction zones, *Nature*, *400*, 443–446.

Bock, Y., L. Prawirodirdjo, J. F. Genrich, C. W. Stevens, R. McCaffrey, C. Subarya, S. S. O. Puntodewo, and E. Calais (2003), Crustal motion in Indonesia from Global Positioning System measurements, *J. Geophys. Res.*, *108*(B8), 2367, doi:10.1029/2001JB000324.

Borrero, J. C., R. Weiss, E. Okal, R. Hidayat, D. A. Suranto, and V. V. Titov (2009), The tsunami of September 12, 2007, Bengkulu Province, Sumatra, Indonesia: Post-tsunami field survey and numerical modeling, *Geophys. J. Int.*, *178*, 180–194.

Briggs, R. W., et al. (2006), Deformation and slip along the Sunda megathrust in the great 2005 Nias-Simeulue earthquake, *Science*, *311*, 1897–1901.

Briggs, R. W., K. Sieh, W. H. Amidon, J. Galetzka, D. Prayudi, I. Suprihanto, N. Sastra, B. Suwargadi, D. Natawidjaja, and T. G. Farr (2008), Persistent elastic behavior above a megathrust rupture patch: Nias island, West Sumatra, *J. Geophys. Res.*, *113*, B12406, doi:10.1029/2008JB005684.

Chlieh, M., J.-P. Avouac, K. Sieh, D. Natawidjaja, and J. Galetzka (2008), Heterogeneous coupling of the Sumatran megathrust constrained by geodetic and paleogeodetic measurements, *J. Geophys. Res.*, *113*, B05305, doi:10.1029/2007JB004981.

Church, J. A., and N. J. White (2006), A 20th century acceleration in global sea-level rise, *Geophys. Res. Lett.*, *33*, L01602, doi:10.1029/2005GL024826.

Church, J. A., N. J. White, R. Coleman, K. Lambeck, and J. X. Mitrovica (2004), Estimates of the regional distribution of sea level rise over the 1950–2000 period, *J. Clim.*, *17*(13), 2609–2625.

Church, J. A., N. J. White, and J. R. Hunter (2006), Sea-level rise at tropical Pacific and Indian Ocean islands, *Global Planet. Change*, *53*(3), 155–168.

Cohen, S. C. (1999), Numerical models of crustal deformation in seismic zones, *Adv. Geophys.*, *41*, 133–231.

DeMets, C., R. G. Gordon, and D. F. Argus (2010), Geologically current plate motions, *Geophys. J. Int.*, *181*, 1–80.

Edwards, R. L., F. W. Taylor, and G. J. Wasserburg (1988), Dating earthquakes with high-precision thorium-230 ages of very young corals, *Earth Planet. Sci. Lett.*, *90*(4), 371–381.

Feng, L., A. V. Newman, M. Protti, V. González, Y. Jiang, and T. H. Dixon (2012), Active deformation near the Nicoya Peninsula, northwestern Costa Rica, between 1996 and 2010: Interseismic megathrust coupling, *J. Geophys. Res.*, *117*, B06407, doi:10.1029/2012JB009230.

Fitch, T. J. (1972), Plate convergence, transcurrent faults, and internal deformation adjacent to Southeast Asia and the Western Pacific, *J. Geophys. Res.*, *77*(23), 4432–4460, doi:10.1029/JB077i023p04432.

Goldfinger, C., et al. (2012), Turbidite event history: Methods and implications for Holocene paleoseismicity of the Cascadia Subduction Zone, *U.S. Geol. Surv. Prof. Pap., 1661-F*, 184 pp.

Goldfinger, C., Y. Ikeda, R. S. Yeats, and J. Ren (2013), Superquakes and supercycles, *Seismol. Res. Lett.*, *84*(1), 24–32.

Gunawan, E., et al. (2014), A comprehensive model of postseismic deformation of the 2004 Sumatra–Andaman earthquake deduced from GPS observations in northern Sumatra, *J. Asian Earth Sci.*, *88*, 218–229.

Hayes, G. P., D. J. Wald, and R. L. Johnson (2012), Slab1.0: A three-dimensional model of global subduction zone geometries, *J. Geophys. Res.*, *117*, B01302, doi:10.1029/2011JB008524.

Hill, E. M., et al. (2012), The 2010 M_w 7.8 Mentawai earthquake: Very shallow source of a rare tsunami earthquake determined from tsunami field survey and near-field GPS, *J. Geophys. Res.*, *117*, B06402, doi:10.1029/2012JB009159.

Hsu, Y.-J., M. Simons, J.-P. Avouac, J. Galetzka, K. Sieh, M. Chlieh, D. Natawidjaja, L. Prawirodirdjo, and Y. Bock (2006), Frictional afterslip following the 2005 Nias-Simeulue earthquake, Sumatra, *Science*, *312*, 1921–1926.

Hsu, Y.-J., M. Simons, C. Williams, and E. Casarotti (2011), Three-dimensional FEM derived elastic Green's functions for the coseismic deformation of the 2005 M_w 8.7 Nias-Simeulue, Sumatra earthquake, *Geochem. Geophys. Geosyst.*, *12*, Q07013, doi:10.1029/2011GC003553.

Jacoby, G. C., P. R. Sheppard, and K. E. Sieh (1988), Irregular recurrence of large earthquakes along the San Andreas Fault; evidence from trees, *Science*, *241*(4862), 196–199.

Jankaew, K., B. F. Atwater, Y. Sawai, M. Choowong, T. Charoentitirat, M. E. Martin, and A. Prendergast (2008), Medieval forewarning of the 2004 Indian Ocean tsunami in Thailand, *Nature*, *455*, 1228–1231, doi:10.1038/nature07373.

Jevrejeva, S., A. Grinsted, J. C. Moore, and S. Holgate (2006), Nonlinear trends and multiyear cycles in sea level records, *J. Geophys. Res.*, *111*, C09012, doi:10.1029/2005JC003229.

Jewell, P. W., and R. L. Bruhn (2013), Evaluation of Wasatch Fault segmentation and slip rates using Lake Bonneville shorelines, *J. Geophys. Res. Solid Earth*, *118*, 2528–2543, doi:10.1002/jgrb.50174.

Kaneko, Y., J.-P. Avouac, and N. Lapusta (2010), Towards inferring earthquake patterns from geodetic observations of interseismic coupling, *Nat. Geosci.*, *3*, 363–369.

Kelleher, J. A. (1972), Rupture zones of large South American earthquakes and some predictions, *J. Geophys. Res.*, *77*(11), 2087–2103, doi:10.1029/JB077i011p02087.

Kemp, A. C., B. P. Horton, J. P. Donnelly, M. E. Mann, M. Vermeer, and S. Rahmstorf (2011), Climate related sea-level variations over the past two millennia, *Proc. Natl. Acad. Sci. U.S.A.*, *108*, 11,017–11,022.

Konca, A. O., V. Hjorleifsdottir, T.-R. A. Song, J.-P. Avouac, D. V. Helmberger, C. Ji, K. Sieh, R. W. Briggs, and A. J. Meltzner (2007), Rupture kinematics of the 2005 M (sub w) 8.6 Nias-Simeulue earthquake from the joint inversion of seismic and geodetic data, *Bull. Seismol. Soc. Am.*, *97*(1A), S307–S322.

Konca, A. O., et al. (2008), Partial rupture of a locked patch of the Sumatra megathrust during the 2007 earthquake sequence, *Nature*, *456*, 631–635.

Kositsky, A. P., and J.-P. Avouac (2010), Inverting geodetic time series with a principal component analysis-based inversion method, *J. Geophys. Res.*, *115*, B03401, doi:10.1029/2009JB006535.

Lay, T., H. Kanamori, C. J. Ammon, K. D. Koper, A. R. Hutko, L. Ye, H. Yue, and T. M. Rushing (2012), Depth-varying rupture properties of subduction zone megathrust faults, *J. Geophys. Res.*, *117*, B04311, doi:10.1029/2011JB009133.

Lohman, R. (2004), The inversion of geodetic data for earthquake parameters, PhD thesis, Calif. Inst. of Technol., Pasadena, Calif.

Loveless, J. P., and B. J. Meade (2010), Geodetic imaging of plate motions, slip rates, and partitioning of deformation in Japan, *J. Geophys. Res.*, *115*, B02410, doi:10.1029/2008JB006248.

Lubis, A. M., A. Hashima, and T. Sato (2013), Analysis of afterslip distribution following the 2007 September 12 southern Sumatra earthquake using poroelastic and viscoelastic media, *Geophys. J. Int.*, *192*(1), 18–37.

McCaffrey, R., P. C. Zwick, Y. Bock, L. Prawirodirdjo, J. F. Genrich, C. W. Stevens, S. S. O. Puntodewo, and C. Subarya (2000), Strain partitioning during oblique plate convergence in northern Sumatra; geodetic and seismologic constraints and numerical modeling, *J. Geophys. Res.*, *105*(B12), 28,363–28,376, doi:10.1029/1999JB900362.

McCann, W. R., S. P. Nishenko, L. R. Sykes, and J. Krause (1979), Seismic gaps and plate tectonics; seismic potential for major plate boundaries, *Pure Appl. Geophys.*, *117*(6), 1082–1147.

Melnick, D., B. Bookhagen, M. R. Strecker, and H. P. Echtler (2009), Segmentation of megathrust rupture zones from fore-arc deformation patterns over hundreds to millions of years, Arauco peninsula, Chile, *J. Geophys. Res.*, *114*, B01407, doi:10.1029/2008JB005788.

Meltzner, A. J., K. Sieh, H.-W. Chiang, C.-C. Shen, B. W. Suwargadi, D. H. Natawidjaja, B. E. Philibosian, R. W. Briggs, and J. Galetzka (2010), Coral evidence for earthquake recurrence and an A.D. 1390–1455 cluster at the south end of the 2004 Aceh-Andaman rupture, *J. Geophys. Res.*, *115*, B10402, doi:10.1029/2010JB007499.

Meltzner, A. J., K. Sieh, H.-W. Chiang, C.-C. Shen, B. W. Suwargadi, D. H. Natawidjaja, B. Philibosian, and R. W. Briggs (2012), Persistent termini of 2004- and 2005-like ruptures of the Sunda megathrust, *J. Geophys. Res.*, *117*, B04405, doi:10.1029/2011JB008888.

Meltzner, A. J., et al. (2014), Similar seismic ruptures and interseismic strain rate variations on the Nias-Simeulue patch of the Sunda megathrust, *Quat. Sci. Rev.*, doi:10.1002/2014JB011200.

Minoura, K., F. Imamura, D. Sugawara, Y. Kono, and T. Iwashita (2001), The 869 Jogan tsunami deposit and recurrence interval of large-scale tsunami on the Pacific coast of Northeast Japan, *J. Nat. Disaster Sci.*, *23*(2), 83–88.

Monecke, K., W. Finger, D. Klarer, W. Kongko, B. G. McAdoo, A. L. Moore, and S. U. Sudrajat (2008), A 1,000-year sediment record of tsunami recurrence in northern Sumatra, *Nature*, *455*(7217), 1232–1234.

Moreno, M., et al. (2011), Heterogeneous plate locking in the South-Central Chile subduction zone: Building up the next great earthquake, *Earth Planet. Sci. Lett.*, *305*, 413–424.

Murtugudde, R., J. P. McCreary, and A. J. Busalacchi (2000), Oceanic processes associated with anomalous events in the Indian Ocean with relevance to 1997–1998, *J. Geophys. Res.*, *105*(C2), 3295–3306, doi:10.1029/1999JC900294.

Natawidjaja, D. H. (2003), Neotectonics of the Sumatran fault and paleogeodesy of the Sumatran subduction zone, PhD thesis, Calif. Inst. of Technol., Pasadena, Calif.

Natawidjaja, D. H., K. Sieh, S. N. Ward, H. Cheng, R. L. Edwards, J. Galetzka, and B. W. Suwargadi (2004), Paleogeodetic records of seismic and aseismic subduction from central Sumatran microatolls, Indonesia, *J. Geophys. Res.*, *109*, 4306, doi:10.1029/2003JB002398.

Natawidjaja, D. H., K. Sieh, M. Chlieh, J. Galetzka, B. W. Suwargadi, H. Cheng, R. L. Edwards, J.-P. Avouac, and S. N. Ward (2006), Source parameters of the great Sumatran megathrust earthquakes of 1797 and 1833 inferred from coral microatolls, *J. Geophys. Res.*, *111*, B06403, doi:10.1029/2005JB004025.

Natawidjaja, D. H., K. Sieh, J. Galetzka, B. W. Suwargadi, H. Cheng, R. L. Edwards, and M. Chlieh (2007), Interseismic deformation above the Sunda megathrust recorded in coral microatolls of the Mentawai islands, West Sumatra, *J. Geophys. Res.*, *112*, B02404, doi:10.1029/2006JB004450.

Newcomb, K. R., and W. R. McCann (1987), Seismic history and seismotectonics of the Sunda Arc, *J. Geophys. Res.*, *92*(B1), 421–439, doi:10.1029/JB092iB01p00421.

Okada, Y. (1992), Internal deformation due to shear and tensile faults in a half-space, *Bull. Seismol. Soc. Am.*, *82*(2), 1018–1040.

Paul, J., A. R. Lowry, R. Bilham, S. Sen, and R. Smalley (2007), Postseismic deformation of the Andaman Islands following the 26 December, 2004 Great Sumatra-Andaman earthquake, *Geophys. Res. Lett.*, *34*, L19309, doi:10.1029/2007GL031024.

Paul, J., C. P. Rajendran, A. R. Lowry, V. Andrade, and K. Rajendran (2012), Andaman postseismic deformation observations: Still slipping after all these years?, *Bull. Seismol. Soc. Am.*, *102*(1), 343–351.

Perfettini, H., and J.-P. Avouac (2014), The seismic cycle in the area of the 2011 M_w9.0 Tohoku-Oki earthquake, *J. Geophys. Res. Solid Earth*, *119*, 4469–4515, doi:10.1002/2013JB010697.

Philibosian, B., T. Fumal, and R. Weldon (2011), San Andreas Fault earthquake chronology and Lake Cahuilla history at Coachella, California, *Bull. Seismol. Soc. Am.*, *101*(1), 13–38.

Philibosian, B., K. Sieh, D. H. Natawidjaja, H.-W. Chiang, C.-C. Shen, B. W. Suwargadi, E. M. Hill, and R. L. Edwards (2012), An ancient shallow slip event on the Mentawai segment of the Sunda megathrust, Sumatra, *J. Geophys. Res.*, *117*, B05401, doi:10.1029/2011JB009075.

Prawirodirdjo, L., R. McCaffrey, C. D. Chadwell, Y. Bock, and C. Subarya (2010), Geodetic observations of an earthquake cycle at the Sumatra subduction zone: Role of interseismic strain segmentation, *J. Geophys. Res.*, *115*, B03414, doi:10.1029/2008JB006139.

Qiu, Q., E. M. Hill, L. Feng, A. M. Lubis, P. Banerjee, J. L. Davis, and K. E. Sieh (2012), "Long-term" post-seismic rate changes detected by the Sumatran GPS Array, western Sumatra, using a Kalman filter, Abstract G43B–0927 presented at 2012 Fall Meeting, AGU, San Francisco, Calif., 3–7 Dec.

Rivera, L., K. Sieh, D. Helmberger, and D. Natawidjaja (2002), A comparative study of the Sumatran subduction-zone earthquakes of 1935 and 1984, *Bull. Seismol. Soc. Am.*, *92*(5), 1721–1736.

Saji, N. H., B. N. Goswami, P. N. Vinayachandran, and T. Yamagata (1999), A dipole mode in the tropical Indian Ocean, *Nature*, *401*, 360–363.

Savage, J. C. (1983), A dislocation model of strain accumulation and release at a subduction zone, *J. Geophys. Res.*, *88*, 4983–4996.

Sawai, Y., M. Shishikura, Y. Okamura, T. Matsu'ura, J. Komatsubara, and T. T. Aung (2007), Tsunami inundation history in Sendai Plain, inferred from tsunami deposits, *Geol. Soc. Am. Abstr. Programs*, *39*(6), 158.

Scoffin, T. P., D. R. Stoddart, and B. R. Rosen (1978), The nature and significance of microatolls, *Philos. Trans. R. Soc. London B*, *284*(999), 99–122.

Shen, C.-C., R. L. Edwards, H. Cheng, J. A. Dorale, R. B. Thomas, S. B. Moran, S. E. Weinstein, and H. N. Edmonds (2002), Uranium and thorium isotopic and concentration measurements by magnetic sector inductively coupled plasma mass spectrometry, *Chem. Geol.*, *185*, 165–178.

Shen, C.-C., et al. (2008), Variation of initial $^{230}Th/^{232}Th$ and limits of high precision U-Th dating of shallow-water corals, *Geochim. Cosmochim. Acta*, *72*(17), 4201–4223.

Shen, C.-C., et al. (2012), High-precision and high-resolution carbonate ^{230}Th dating by MC-ICP-MS with SEM protocols, *Geochim. Cosmochim. Acta*, *99*, 71–86.

Sieh, K., S. N. Ward, D. Natawidjaja, and B. W. Suwargadi (1999), Crustal deformation at the Sumatran subduction zone revealed by coral rings, *Geophys. Res. Lett.*, *26*(20), 3141–3144, doi:10.1029/1999GL005409.

Sieh, K., D. H. Natawidjaja, A. J. Meltzner, C.-C. Shen, H. Cheng, K.-S. Li, B. W. Suwargadi, J. Galetzka, B. Philibosian, and R. L. Edwards (2008), Earthquake supercycles inferred from sea-level changes recorded in the corals of west Sumatra, *Science*, *322*, 1674–1678.

Taylor, F. W., C. Frohlich, J. Lecolle, and M. R. Strecker (1987), Analysis of partially emerged corals and reef terraces in the central Vanuatu Arc: Comparison of contemporary coseismic and nonseismic with Quaternary vertical movements, *J. Geophys. Res.*, *92*(B6), 4905–4933, doi:10.1029/JB092iB06p04905.

Thatcher, W. (1984), The earthquake deformation cycle, recurrence, and the time-predictable model, *J. Geophys. Res.*, *89*(B7), 5674–5680, doi:10.1029/JB089iB07p05674.

Vergne, J., R. Cattin, and J.-P. Avouac (2001), On the use of dislocations to model interseismic strain and stress build-up at intracontinental thrust faults, *Geophys. J. Int.*, *147*(1), 155–162.

Wang, K., Y. Hu, and J. He (2012), Deformation cycles of subduction earthquakes in a viscoelastic Earth, *Nature*, *484*(7394), 327–332.

Webster, P. J., A. M. Moore, J. P. Loschnigg, and R. R. Leben (1999), Coupled ocean-atmosphere dynamics in the Indian Ocean during 1997–98, *Nature*, *401*(6751), 356–360.

Weldon, R., K. Scharer, T. Fumal, and G. Biasi (2004), Wrightwood and the earthquake cycle: What a long recurrence record tells us about how faults work, *GSA Today*, *14*(9), 4–10.

Woodworth, P. L., and R. Player (2003), The permanent service for mean sea level: An update to the 21st century, *J. Coast. Res.*, *19*(2), 287–295.

Zachariasen, J., K. Sieh, F. W. Taylor, R. L. Edwards, and W. S. Hantoro (1999), Submergence and uplift associated with the giant 1833 Sumatran subduction earthquake: Evidence from coral microatolls, *J. Geophys. Res.*, *104*(B1), 895–919, doi:10.1029/1998JB900050.

Zachariasen, J., K. Sieh, F. W. Taylor, and W. S. Hantoro (2000), Modern vertical deformation above the Sumatran subduction zone: Paleogeodetic insights from coral microatolls, *Bull. Seismol. Soc. Am.*, *90*(4), 897–913.

Zweck, C., J. Freymueller, and S. C. Cohen (2002), Three-dimensional elastic dislocation modeling of the postseismic response to the 1964 Alaska earthquake, *J. Geophys. Res.*, *107*(B4), 2064, doi:10.1029/2001JB000409.